10

Phase Transformations and Recrystallization Processes During Synthesis, Processing and Service of TiAl Alloys

Fritz Appel
Institute for Materials Research, Helmholtz-Zentrum Geesthacht, Geesthacht, Germany

1. Introduction

Titanium aluminides alloys based on the intermetallic phases $\alpha_2(Ti_3Al)$ and $\gamma(TiAl)$ are one of the few classes of emerging materials that have the potential for innovative applications in advanced energy conversion systems whenever low density, good high-temperature strength and resistance against ignition and corrosion are of major concern [1]. The outstanding thermo-physical properties of the individual phases mainly result from the highly ordered nature and directional bonding of the compounds. However, two-phase $\alpha_2(Ti_3Al)+\gamma(TiAl)$ alloys exhibit a much better mechanical performance than their monolithic constituents $\gamma(TiAl)$ and $\alpha_2(Ti_3Al)$, provided that the phase distribution and grain size are suitably controlled. The synergistic effects of the two phases are undoubtedly associated with the many influences that the microstructure has on deformation and fracture processes. Constitution and microstructure are the result of phase transformations, ordering reactions and recrystallization processes, which occur during synthesis, processing and service. Many aspects of these mechanisms are intimately linked to defect configurations at the atomic level; thus standard techniques of metallography were often inadequate to provide the necessary information. This lack of information is addressed in the present article in that observations on recrystallization and phase transformations by high-resolution electron microscopy are presented. Particular emphasis will be paid on

i. the origin of microstructures
ii. heterogeneities in the deformed state and recovery behaviour
iii. atomic structure of crystalline and crystalline/amorphous interfaces
iv. misfit accommodation and coherency stresses.

2. Constitution and microstructure

2.1 Constitution

TiAl alloys of technical significance have the general composition (in at. %, as are all compositions in this paper)

$$\text{Ti-(42-49)Al+X}, \tag{1}$$

with X designating alloying elements, such as Cr, Nb, W, V, Ta, Si, B, and C [2]. When referred to the binary phase diagram (Fig. 1), the equilibrium phases for Al contents between 46 and 49 % are: the disordered solution phases hexagonal (h.c.p.) α(Ti), body centred cubic (b.c.c.) β(Ti), and the ordered intermetallic compounds γ(TiAl) with $L1_0$ structure, and $\alpha_2(Ti_3Al)$ with $D0_{19}$ structure [3]. Based on this constitution, different microstructures have been designed. The phase transformations involved in the microstructural evolution will be demonstrated for two examples, the classical lamellar structure of $\alpha_2(Ti_3Al)+\gamma(TiAl)$ alloys and a novel crystallographically modulated morphology occurring in multiphase alloys.

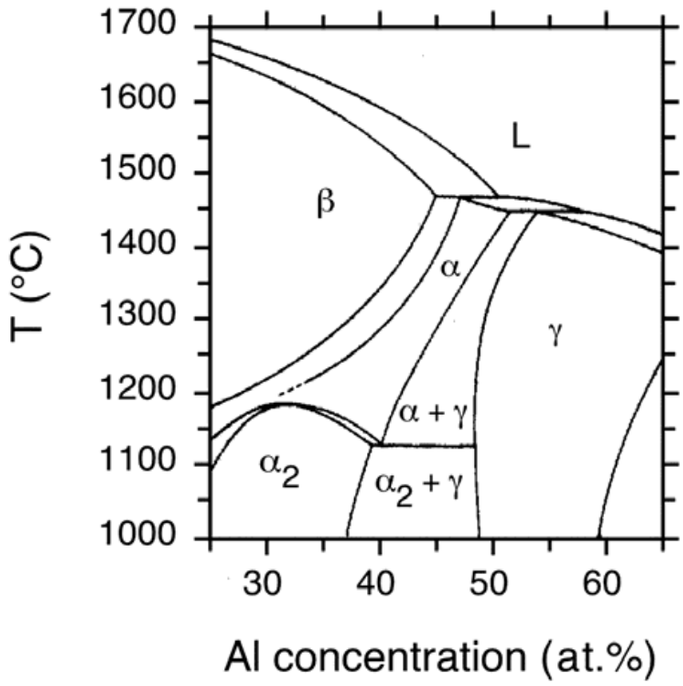

Fig. 1. Central portion of the Ti-Al-phase diagram in the region of technical interest [3].

2.2 Lamellar microstructure

The technologically most relevant $\alpha_2(Ti_3Al)+\gamma(TiAl)$ alloys contain a significant volume fraction of lamellar grains [1, 2]. The morphology of these grains represents a multilayer system made of two phases. It is well documented in the literature [4] that such a system could exhibit extraordinary mechanical properties when the layer thickness is small enough.

The so-called lamellar microstructure results from the precipitation of γ lamellae in either a disordered α or a congruently ordered α_2' matrix, following one of the transformation paths [3]:

$$\alpha \rightarrow \alpha_2' \rightarrow \alpha_2+\gamma \text{ or } \alpha \rightarrow \alpha_2+\gamma. \quad (2)$$

α_2' and α_2 have the same crystal structure but different composition. The exact pathway is still a matter of debate and could depend on alloy composition and thermal treatment. The orientation relationships between the α_2 and γ platelets are [5]

$$\{111\}\gamma \,||\, (0001)\alpha 2 \text{ and } [1\,\bar{1}\,0]\gamma \,||\, <11\,\bar{2}\,0>\alpha 2. \quad (3)$$

The length of the lamellae is determined by the size of the parent α/α_2 grain. The γ phase is formed as an ordered domain structure, as sketched in Fig. 2. This gives rise to six variants of the above orientation relationships. Thus, there are four types of lamellar interfaces: the α_2/γ interface and three distinct γ/γ interfaces that are typified by rotations of 60°, 120° and 180° between adjacent lamellae. A lamellar grain consists of a set of γ lamellae, which are subdivided into domains and interspersed by α_2 lamellae. The volume fraction of the two phases is controlled by the composition on the basis of the phase diagram and the processing conditions of the alloy. However, it should be noted that the decomposition of α phase into lamellar ($\alpha_2+\gamma$) is sluggish and often cannot be established within the constraints of processing routes; thus the volume fraction of γ phase is less than equilibrium [6]. It might be expected that the Ti concentration in the γ phase increases when the alloy becomes richer in Ti until the maximum solubility of Ti in the γ phase is reached. This non-equilibrium phase composition may provide significant driving forces for structural changes, as will be outlined in the subsequent sections.

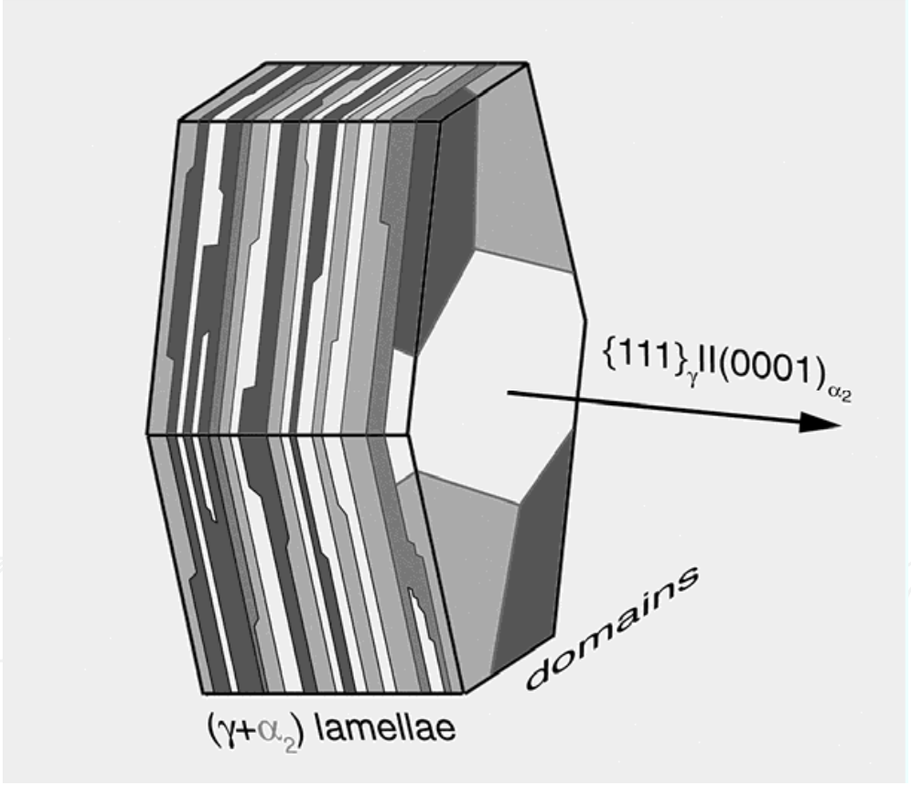

Fig. 2. Schematic drawing of a lamellar colony comprised of γ and α_2 platelets.

Among the various lamellar interfaces only the twin boundary is fully coherent, as the adjacent lattices are symmetrically oriented. At all the other interfaces the matching is imperfect, i.e., these interfaces are semicoherent. The mismatch arises from the differences in the crystal structure and lattice parameters and amounts to 1 to 2 %, depending on alloy composition and processing conditions. Different modes of mismatch accommodation have

been discussed for lamellar TiAl alloys, which in broad terms correspond to the early models of misfitting interfaces [7]. Up to a certain point, the misfit strain could be solely taken up by elastic distortion, i.e., the lamellae are uniformly strained to bring the atomic spacings into registry. This homogeneous strain accommodation leads to coherent interfaces but introduces lattice distortions that are known as coherency strains. Hazzledine [4] has shown that the elastic misfit accommodation in lamellar ($\alpha_2+\gamma$) alloys is only possible if the lamellae are very thin. The predicted critical thicknesses are $d_c \leq 8$ nm for the mismatched γ/γ interfaces and $d_c \leq 0.8$ to 3.9 nm for the α_2/γ interfaces, depending on the volume content of α_2 phase. Figure 3 shows a small Ti_3Al platelet embedded in γ phase with a thickness of 4.5 nm, which is just above the coherency limit predicted by Hazzledine [4]. While homogeneous strain accommodation is still recognizable, part of the misfit is already taken up by interfacial defects.

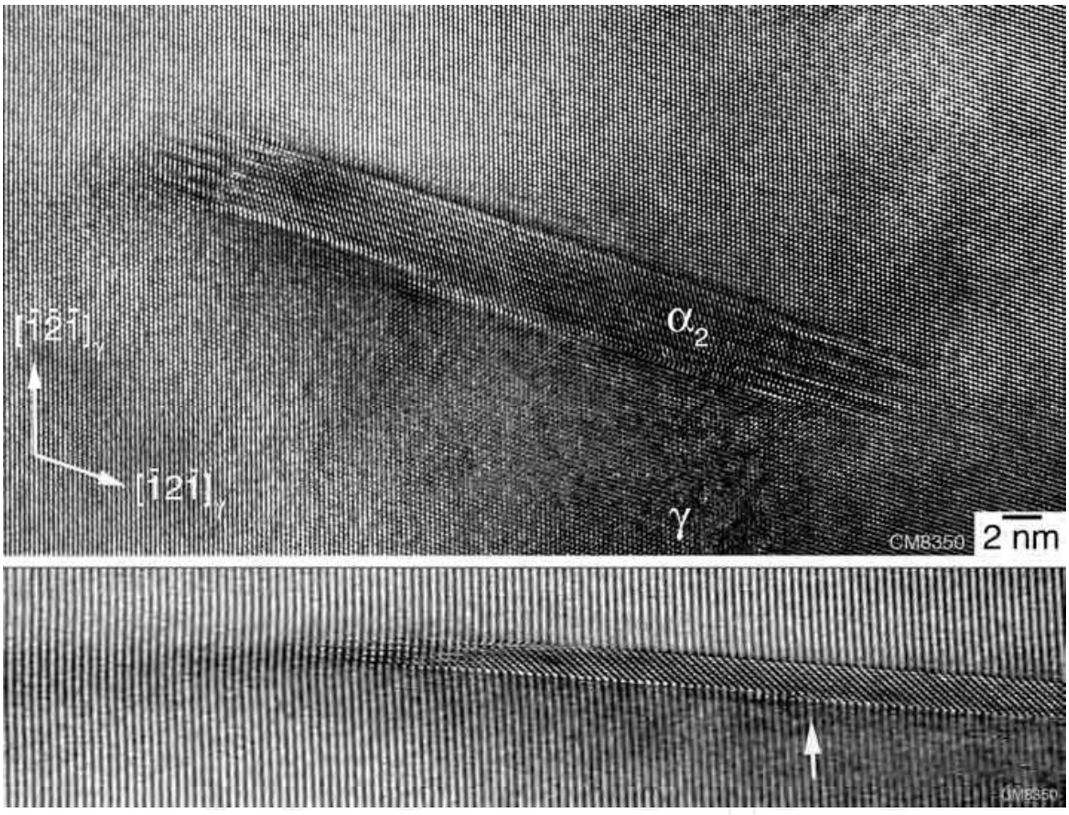

Fig. 3. High-resolution electron micrograph showing a small Ti_3Al platelet embedded in γ phase. Interfacial steps, dislocations and homogeneous elastic straining accommodate the misfit between the particle and the matrix. In the compressed image below, the elastic straining at the tip of the particle is readily visible by the distortion of the $(\bar{1}1\bar{1})$ planes. A dislocation compensating the misfit between the $(\bar{1}1\bar{1})_\gamma$ and $\{2\bar{2}01\}_{\alpha 2}$ planes is arrowed. Ti-46.5Al-4(Cr, Ta, Mo, B), sheet material.

The coherency strains raise the total energy of the system. Thus, for a sufficiently large misfit, or lamellar spacing, it becomes energetically more favourable to replace the coherent interface by a semicoherent interface, a situation that is referred to as a loss of coherency. As

described in the early model of Frank and van der Merve [8] misfit dislocations partially take up the misfit, i.e., the atoms at the interface adjust their positions to give regions of good and bad registry. In other words, the misfit is concentrated at the dislocations.

Mismatch strains at interfaces can be also relieved by the formation of ledges or steps at the interface [9]. The introduction of mono-atomic steps significantly improve the atomic matching, thus preventing the disregistry from becoming large anywhere. Structural ledges may replace misfit dislocations as a way of retaining low-index terraces between the respective defects. The general view is that planar boundaries are favoured for large misfits and small Burgers vectors of the misfit dislocations, whereas stepped boundaries are favoured for small misfits and large values of the Burgers vector. Steps may range in scale from atomic to multi-atomic dimensions depending on energetic or kinetic factors. However, it is very often the case that an interfacial defect exhibits both dislocation- and step-like character, thus, comprising a more general defect that has been defined as a disconnection [10,11]. Because of its step character, disconnection motion along an interface transports material from one phase to the other, the extent of which is essentially determined by the step height. At the same time, the dislocation content of the disconnection leads to deformation. In this sense, disconnection motion couples interface migration with deformation. The different extents of symmetry breaking at the interfaces lead to a broad variety of disconnections [10, 11]. This is reflected in different step heights and dislocation contents, which eventually determine the function of disconnections in phase transformations. Disconnection models have been developed for a variety of diffusional and diffusionless phase transformations in crystalline solids; and an extensive body of literature has evolved. For more details the reader is referred to a review of Howe et al. [11]. Several authors [12-16] observed interfacial steps at α_2/γ interfaces with heights that were always a multiple of $\{111\}_\gamma$ planes. The most commonly observed two-plane steps were characterized as disconnections with the topological parameters $b=1/6[11\bar{2}]$, $t(\gamma)=1/2[\overline{11}2]_\gamma$ and $t(\alpha_2)=[000\bar{1}]_{\alpha 2}$ [17]. b is the Burgers vector of the dislocation component (parallel to the (111) interface) and $t(\gamma)$ and $t(\alpha_2)$ are vectors describing the ledge risers [11] of the disconnection. This type of disconnection has no Burgers vector component perpendicular to the interface.

The complexity of misfit accommodation at α_2/γ interfaces is illustrated in Fig. 4. The micrograph shows a γ(TiAl) lamella terminated within the α_2 phase of a two-phase alloy. The interface marked in the micrograph borders the crystal region in which the exact *ABC* stacking of the $L1_0$ structure is fulfilled. Outside of this exactly stacked region of γ phase, there is a two to three atomic plane thick layer in which neither the *ABC* stacking of the γ phase nor the *ABAB* stacking of the α_2 phase is correctly fulfilled. This becomes particularly evident at the tip of the γ lamellae and indicates a significant homogeneous straining of the lattice. This strain seems to locally relax by the formation of dislocations, as can be seen in the compressed form of the image. The other salient feature is the misfit accommodation by steps. A Burgers circuit constructed around the tip of the γ lamella results in a projected Burgers vector of $b_p=1/6[11\bar{2}]$. This indicates that the small misfit between the $(111)_\gamma$ and $(0002)_{\alpha 2}$ planes is elastically taken up. The observed misfit accommodation is pertinent to the issue of how differential material flux during the $\alpha_2 \rightarrow \gamma$ transformation is accomplished.

There is ample evidence [18] of enhanced self-diffusion along dislocation cores. Likewise interfacial ledges are envisaged as regions where deviation from the ideal structure is localized and which may provide paths of easy diffusion. This gives rise to the speculation that it is mainly the tip of a newly formed γ lamella where the atomic composition between the two phases is adjusted during transformation.

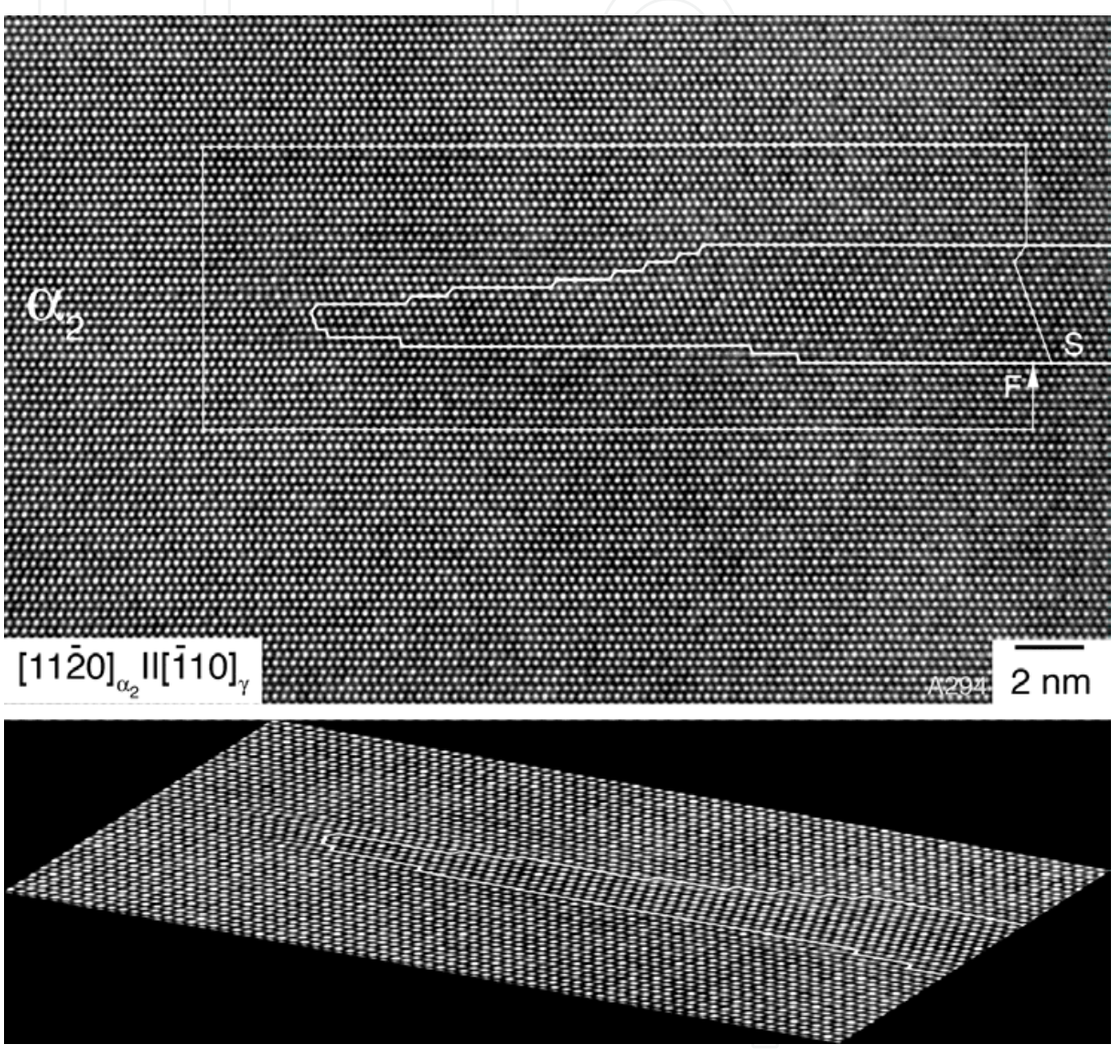

Fig. 4. A high-resolution micrograph of a γ(TiAl) lamella terminated within α_2 phase imaged down the $<10\,\bar{1}>_{\gamma}$ and $<11\,\bar{2}\,0>_{\alpha 2}$ directions. The thick white line marks the position of the interface. The salient feature is the misfit accommodation by steps. S and F denote the start and finish, respectively, of the Burgers circuit constructed around the tip of the γ lamella. After elimination of all the cancelling components in the initial circuit, and transforming the sequence of operations in the α_2 phase into the γ coordinate frame, the projected Burgers vector is $b_p=1/6[\,11\bar{2}\,]$. Note the dislocation in front of the γ tip. This can be recognized in the image below, which was compressed along the $(\,2\bar{2}01\,)_{\alpha 2}$ planes. Ti-Al-Nb, as cast.

In spite of the misfit accommodation by interfacial dislocations and ledges a significant elastic strain remains at the interfaces. The resulting coherency stresses were determined by convergent beam electron diffraction (CBED) [19] and by analyzing the configuration of dislocations emitted from the lamellar interfaces [20]. The investigations have shown that the residual coherency stresses are comparable with the yield stress of the material. From theory it is expected that the residual coherency stresses present in the individual lamellae are inversely proportional to the lamellar spacing λ_L [21]. However, when sampled over a sufficiently large volume, the average of the coherency strain was zero. Thus, the sign of the coherency strain alternates from lamella to lamella. In the design of lamellar alloys λ_L is often reduced in order to maximize the yield stress. At the same time the coherency stresses grow both in absolute magnitude and relative to the yield stress [4]. Thus, in high-strength alloys the coherency stresses can be very large and can affect deformation, phase transformations, recovery, and recrystallization in various ways, as will be described in the following sections.

2.3 Modulated microstructures

In an attempt to improve the balance of mechanical properties, a novel type of TiAl alloys, designated γ-Md, with a composite-like microstructure has been recently developed [22]. The design bases on the general composition

$$\text{Ti-(40-44)Al-8.5 Nb.} \tag{4}$$

The characteristic constituents of the alloy are laths with a modulated substructure that is comprised of stable and metastable phases. The modulation occurs at the nanometer scale and thus provides an additional structural feature that refines the material. As indicated by X-ray analysis the constitution of the alloys (4) involves the β/B2, α_2 and γ phases. Additional X-ray reflections could be attributed to the presence of two orthorhombic phases with B19 structure, (oP4, Pmma and oC16, Cmcm). However, a clear association with the various orthorhombic structures reported in the literature was not possible because of their structural similarity. It might be expected that the evolution of the constitution does not reach thermodynamic equilibrium; thus, the number of the transformation products may be larger than expected from the phase rule. The microstructure of the alloy is shown in Fig. 5. The characteristic features are laths with a periodic variation in the diffraction contrast, which intersperse the other constituents. As shown in Fig. 5a, the contrast fluctuations occur at a very fine length scale. The evidence of the high-resolution electron microscope observations is that a single lath is subdivided into several regions with different crystalline structures with no sharp interface in between. The high-resolution micrograph in Fig. 5b shows a lath adjacent to a γ lamella in $<101]_\gamma$ projection, which can be used as a reference. The interface between the lath and the γ phase (designated as γ/T) consists mainly of flat terraces, which are parallel to the $(111)_\gamma$ plane. Steps of different heights often delineate the terraces. The modulated laths are comprised of an orthorhombic constituent, which is interspersed by slabs of β/B2 and a little α_2 phase (Fig. 6). Selected area diffraction of the orthorhombic constituent is consistent with the B19 phase, which can be described as the orthorhombic phase (oP4) or as a hexagonal superstructure of $D0_{19}$ (hP8). In the Ti-Al system, the B19 structure has already been observed by Abe et al. [23] and Ducher et al. [24]. The B19 structure is structurally closely related to the orthorhombic phase (oC16, Cmcm) with the ideal stoichiometry Ti_2AlNb, which among the intermetallic compounds is remarkable for its relatively good room temperature ductility [25].

In Figs. 5b and 6a the B19 structure is imaged in the $[010]_{B19}$ projection. As deduced from the high-resolution images, the orientation relationships between the constituents involved in a modulated lath with the adjacent γ are [22]

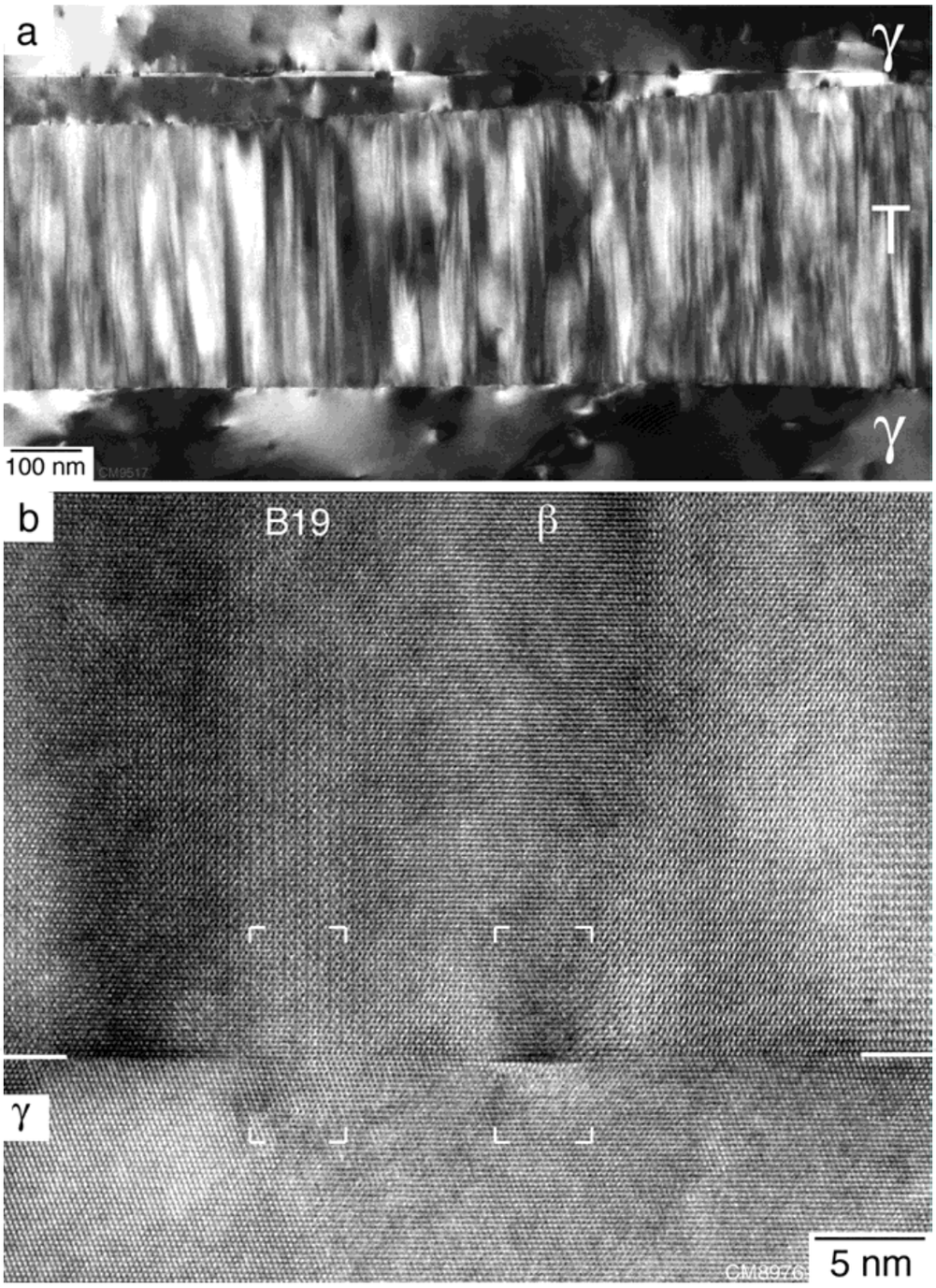

Fig. 5. TEM analysis of the modulated microstructure. (a) A modulated lath imaged by diffraction contrast. (b) High-resolution TEM micrograph of a modulated lath adjacent to a γ lamella.

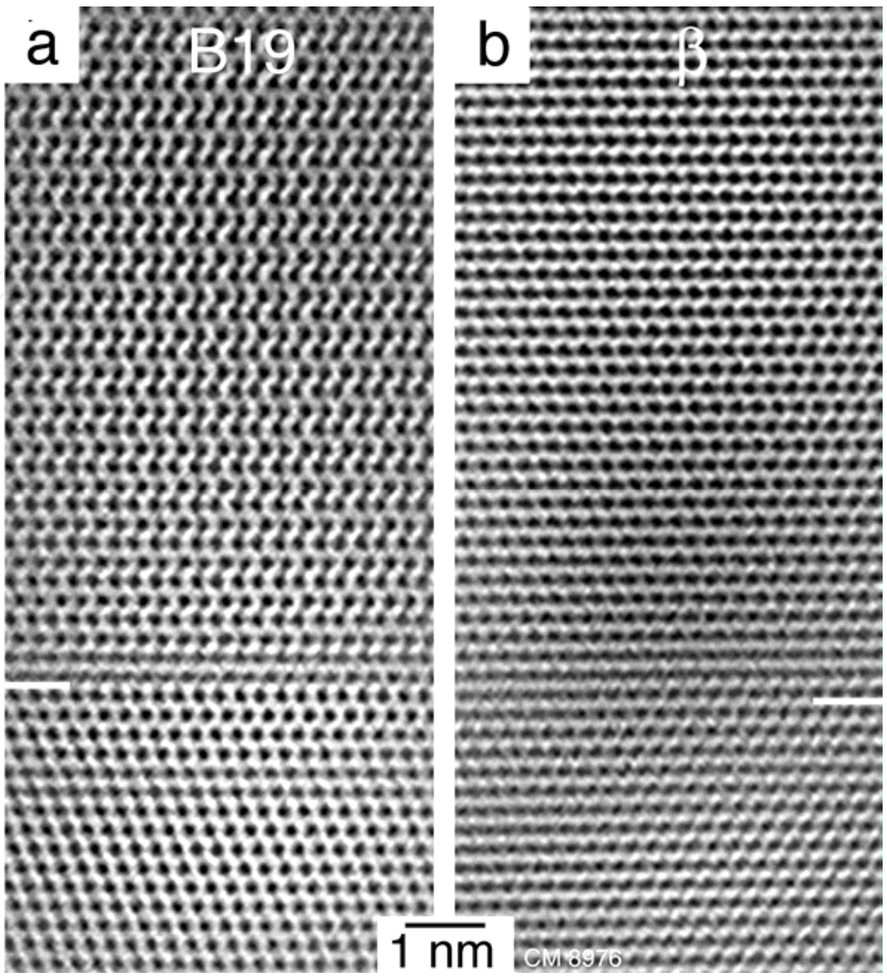

Fig. 6. High-resolution TEM evidence of the modulated microstructure. (a) and (b) Fourier-filtered images of the areas boxed in Fig. 5.

$$(100)_{B19} \,||\, \{110\}_{\beta/B2} \,||\, (0001)_{\alpha 2} \,||\, \{111\}_{\gamma}$$
$$[010]_{B19} \,||\, \langle 111\rangle_{\beta/B2} \,||\, \langle 11\bar{2}0\rangle_{\alpha 2} \,||\, \langle 1\bar{1}0\rangle_{\gamma};\ [001]_{B19} \,||\, \langle 11\bar{2}\rangle_{\gamma}. \quad (5)$$

In the diffraction pattern the presence of the periodic distortion is manifested by the existence of weak satellite reflections adjacent to the main reflections. The distance of the satellites from the main reflections is the reciprocal of the modulation wavelength, and the direction joining the satellites with their main reflections is parallel to the direction of the modulation vector. These observed features are reminiscent of a modulated structure, which in recent years have attracted considerable interest; for a review see [26]. A crystal structure is said to be modulated if it exhibits periodicities other than the Bravais lattice periodicities. These additional periodicities arise from one or more distortions, which increase to a maximum value and then decrease to the initial value. The modulation may involve atomic coordinates, occupancy factors or displacement parameters. The strain of the discontinuities is often relieved by a continuous and periodic variation of the physical properties of the

product. First principle calculations of Nguyen-Manh and Pettifor [27] and Yoo and Fu [28] have shown that the β/B2 phase existing in TiAl alloys containing supersaturations of transition metals (Zr, V, Nb) is unstable under tetragonal distortion; a shear instability that was attributed to the anomalous (negative) tetragonal shear modulus. Specifically, B2 may transform by homogeneous shear to several low temperature orthorhombic phases, which can exist metastably. The energetically favourable transformations are [27]

$$\mathrm{B2(Pm3m)} \rightarrow \mathrm{B19(Pmma)} \rightarrow \mathrm{B33(Cmcm)}. \quad (6)$$

At the atomic level, the B2 phase may transform to B19 by a shuffle displacement of neighboring $(011)_{B2}$ planes in opposite $[01\bar{1}]$ directions, as illustrated in Fig. 7. A subsequent displacement of neighboring $(011)_{B2}$ planes in the [100] direction generates the B33 structure [27]. In the system investigated here the predominant orthorhombic phase seems to be B19. It is tempting to speculate that the modulation of the laths is triggered by a periodic variation of the composition of the parent B2 phase, as occurs during spinodal decomposition. Clearly the mechanism requires further investigation.

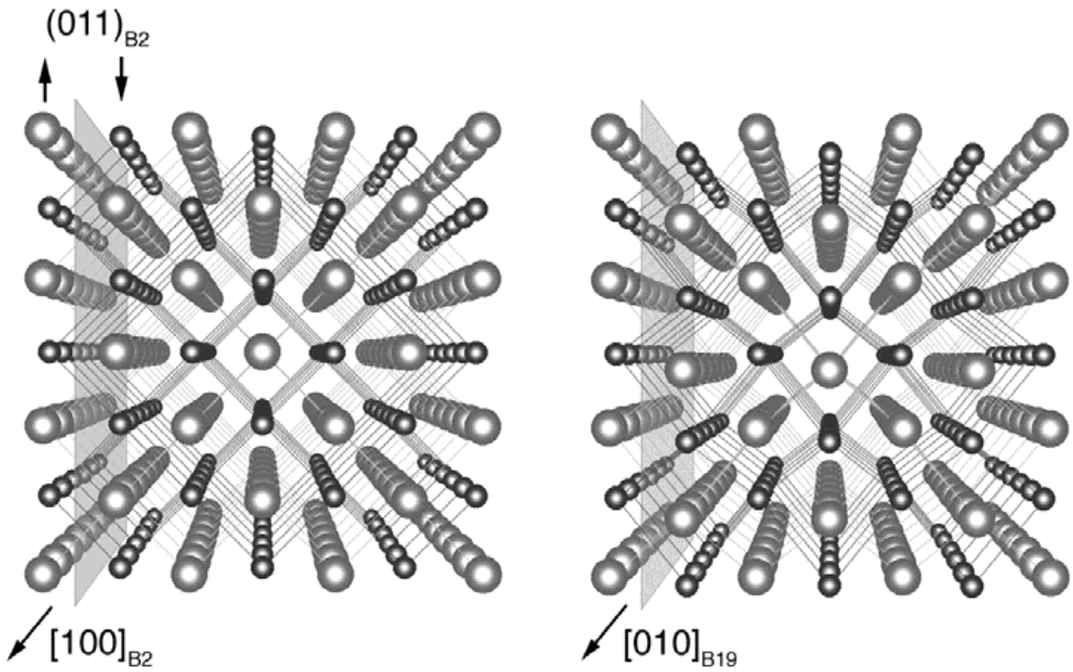

Fig. 7. Formation of the B19 structure from the parent B2 phase illustrated by perspective views of hard-sphere models. [100] projection of the B2 phase; arrow heads mark shuffle displacements of neighbouring $(011)_{B2}$ planes in opposite $[01\bar{1}]$ directions to form B19.

The modulated laths can apparently further transform into the γ phase, as demonstrated in Fig. 8. This process often starts at grain boundaries and proceeds through the formation of high ledges via distinct atomic shuffle displacements. As this transformation was frequently observed in deformed samples [22], it might be speculated that the process is stress induced and provides some kind of transformation toughening.

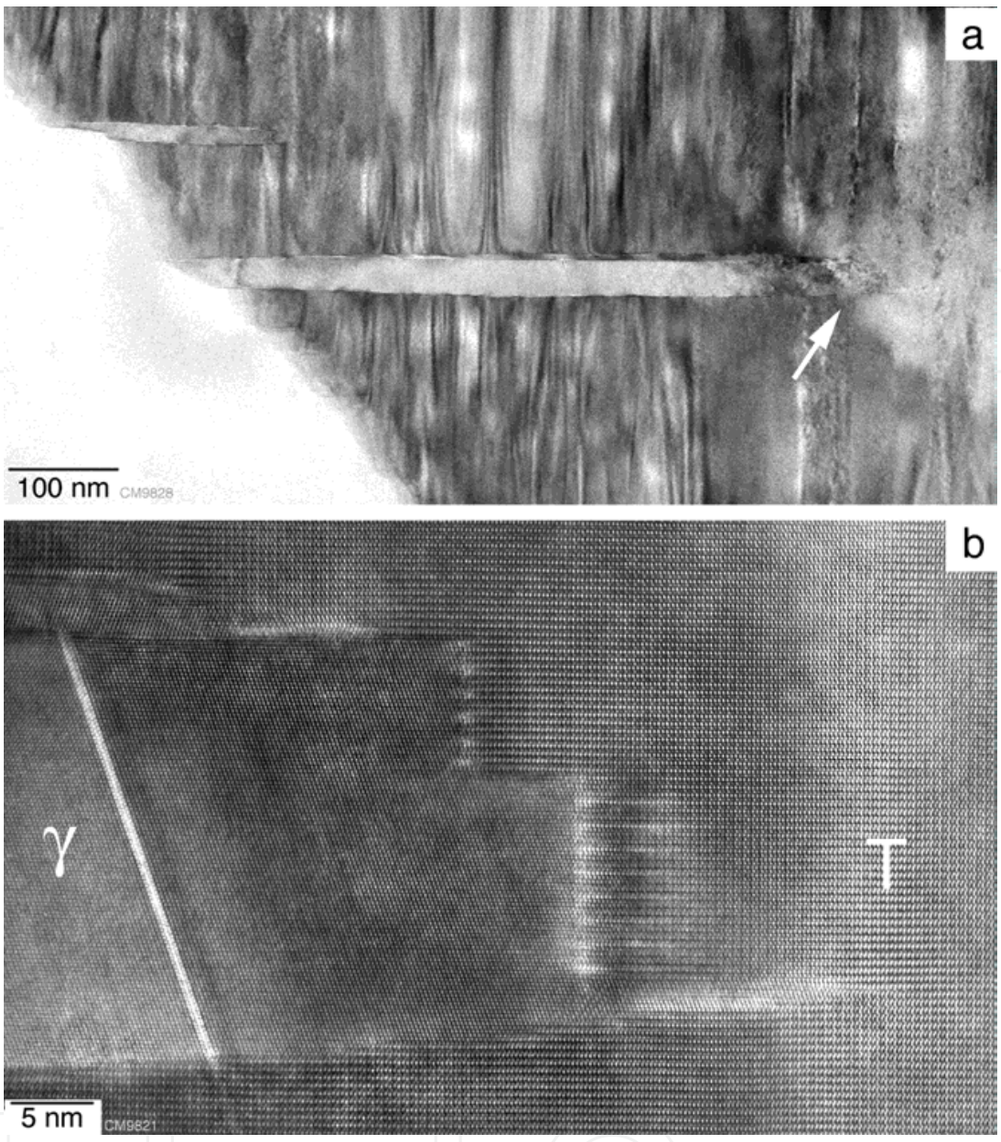

Fig. 8. Stress-induced transformation of a modulated lamella (T) into γ phase. (a) Generation of a γ lamella at a grain boundary. (b) Higher magnification of the area marked by the arrow in (a). Note the ledges at the interfaces.

3. Hot working

Titanium aluminide alloys are relatively brittle materials; attaining chemical homogeneity and refinement of the microstructure are therefore the most important prerequisites for engineering applications. To this end, large effort has been expended to establish wrought processing of TiAl alloys [29, 30]. Hot working of these alloys is generally impeded by a significant plastic anisotropy [31], low diffusivity [32] and the susceptibility to hot cracking [29]. While these aspects are well documented in the TiAl literature, there are many open questions about the elementary processes that determine dynamic recovery, recrystallization and phase transformations. These aspects are addressed in the present section.

3.1 The deformed state

A commonly held concept of hot working is that dynamic recovery and recrystallization are triggered by heterogeneities in the deformed state. Thus, the deformation mechanisms occurring in the majority phases γ(TiAl) and α_2(Ti_3Al) will briefly be discussed, for details see [1, 31]. Deformation of γ(TiAl) is mainly provided by ordinary dislocations with the Burgers vector b=1/2<110] and mechanical twinning along $1/6<11\bar{2}]\{111\}$. Since twinning shear is unidirectional, the operating twinning systems vary with the sense of the load and the loading direction. There are crystal orientations for which twinning is forbidden. To a lesser extent deformation is provided by the motion of superdislocations with the Burgers vectors b=<101] and $b=1/2<11\bar{2}]$. The superdislocations exhibit an asymmetric non-planar core spreading; this results in a high glide resistance, which is sensitive to the direction of motion, for a review see [33]. Thus, the superdislocations do not move as readily as ordinary dislocations and mechanical twins. Taken together, this glide geometry gives rise to a significant plastic anisotropy of the γ phase. Ti_3Al alloys have several potential slip systems, which in principle may provide sufficient shear components for the deformation of polycrystalline material. However, there is a strong predominance for prismatic slip; plastic shear with c components of the hexagonal cell is practically impossible [34]. This plastic anisotropy appears to be even more enhanced at intermediate temperatures because the pyramidal slip systems exhibit an anomalous increase of the critical resolved shear stress with temperature. Thus, the brittleness of polycrystalline Ti_3Al alloys can be attributed to the lack of independent slip systems that can operate at comparable stresses; hence the von Mises criterion is not satisfied. Due to this situation deformation of γ(TiAl)+α_2(Ti_3Al) alloys is mainly carried by the γ phase.

There are various processes that might lead to heterogeneities in the deformed state. As a specific example for TiAl alloys, deformation heterogeneities resulting from mechanical twinning will be outlined in more detail. At the beginning of deformation the slip path of the twins is essentially identical with the domain size or lamellar spacing. As soon as multiple twinning with non-parallel shear vectors is activated, extensive intersections among twin bands occur. The intersection of a moving deformation twin with a barrier twin is expected to be difficult because the incorporation of an incident twinning system into the barrier twin may no longer constitute a crystallographically allowed twinning system. Several authors [35-39] have analyzed the mechanism and have proposed crystallographic relations by which an incident twin could intersect a barrier twin. The high-resolution electron micrograph shown in Fig. 9 demonstrates a so-called type-I twin intersection, which is favoured if the $<\bar{1}10]$ intersection line is at 0° to 55° from the sample axis [35]. The structure is imaged along the common $<\bar{1}10]$ direction of the two twins; this can be recognized by the different contrast of the (002) planes, which are alternately occupied by Ti and Al atoms. On its upper side the vertical twin is thicker than on its lower side, thus this twin was considered as incident twin T_i; T_b is the barrier twin. The intersection leads to a significant deflection of the two twins, which, however, is more pronounced for the barrier twin. The difficulty in forming a twin intersection is manifested by the ledged interface between the incident twin and the matrix (arrows 1 and 3) and various dislocations that emerge at the intersection zone (arrows 2). Figure 10 shows the details of the intersection zone. The intersection zone remains in the $L1_0$ structure and seems to be relatively free of defects; however highly defective regions border it. The $(002)_{Tb}$ planes of the central zone

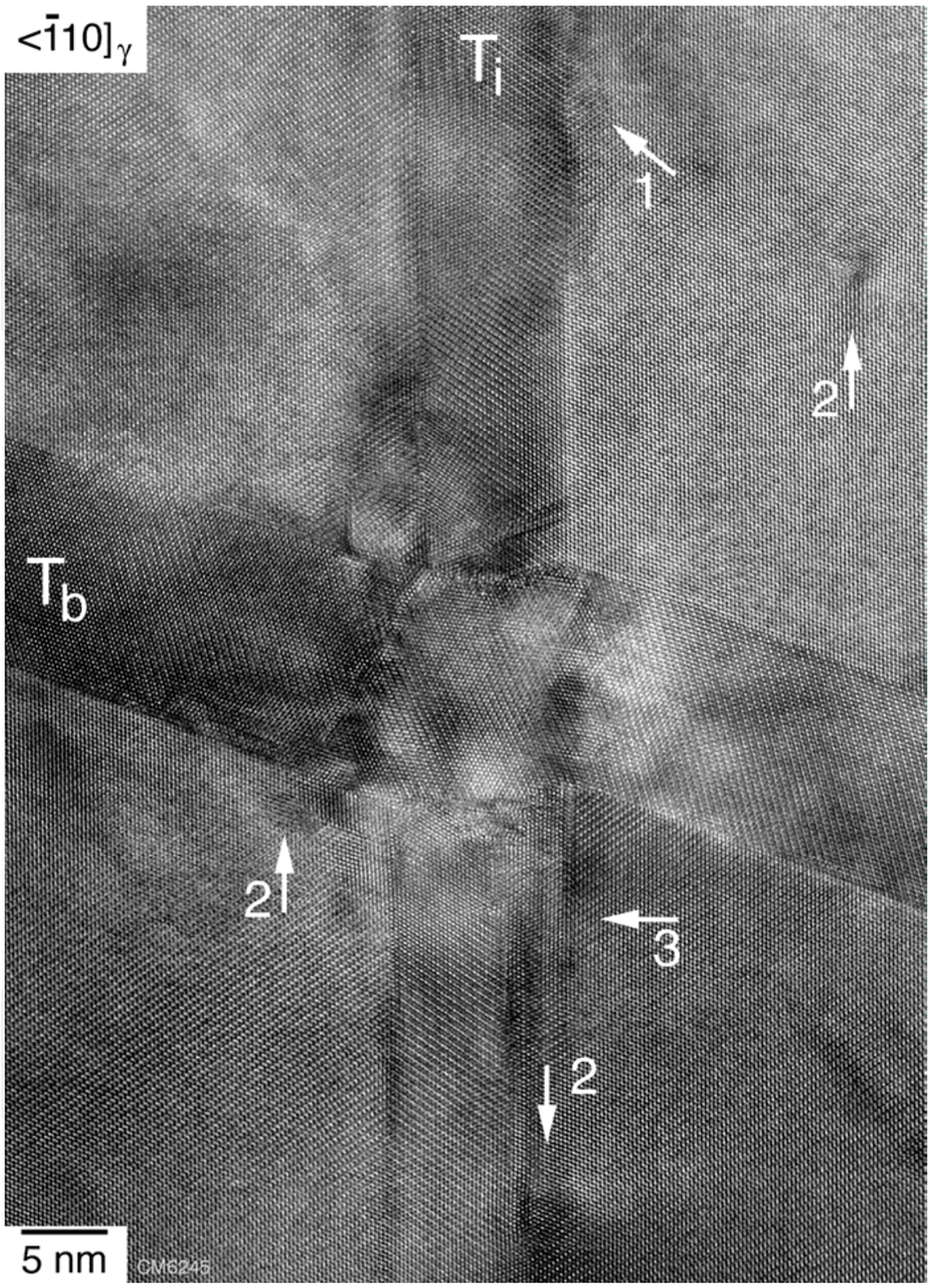

Fig. 9. Type-I intersection of two deformation twins observed after room temperature compression of a Ti-48.5Al-0.37C alloy. The structure is imaged along the common < $\bar{1}$10] intersection line. The vertical twin T_i is considered to be the incident twin because its upper side is thicker than its lower side; T_b is the barrier twin.

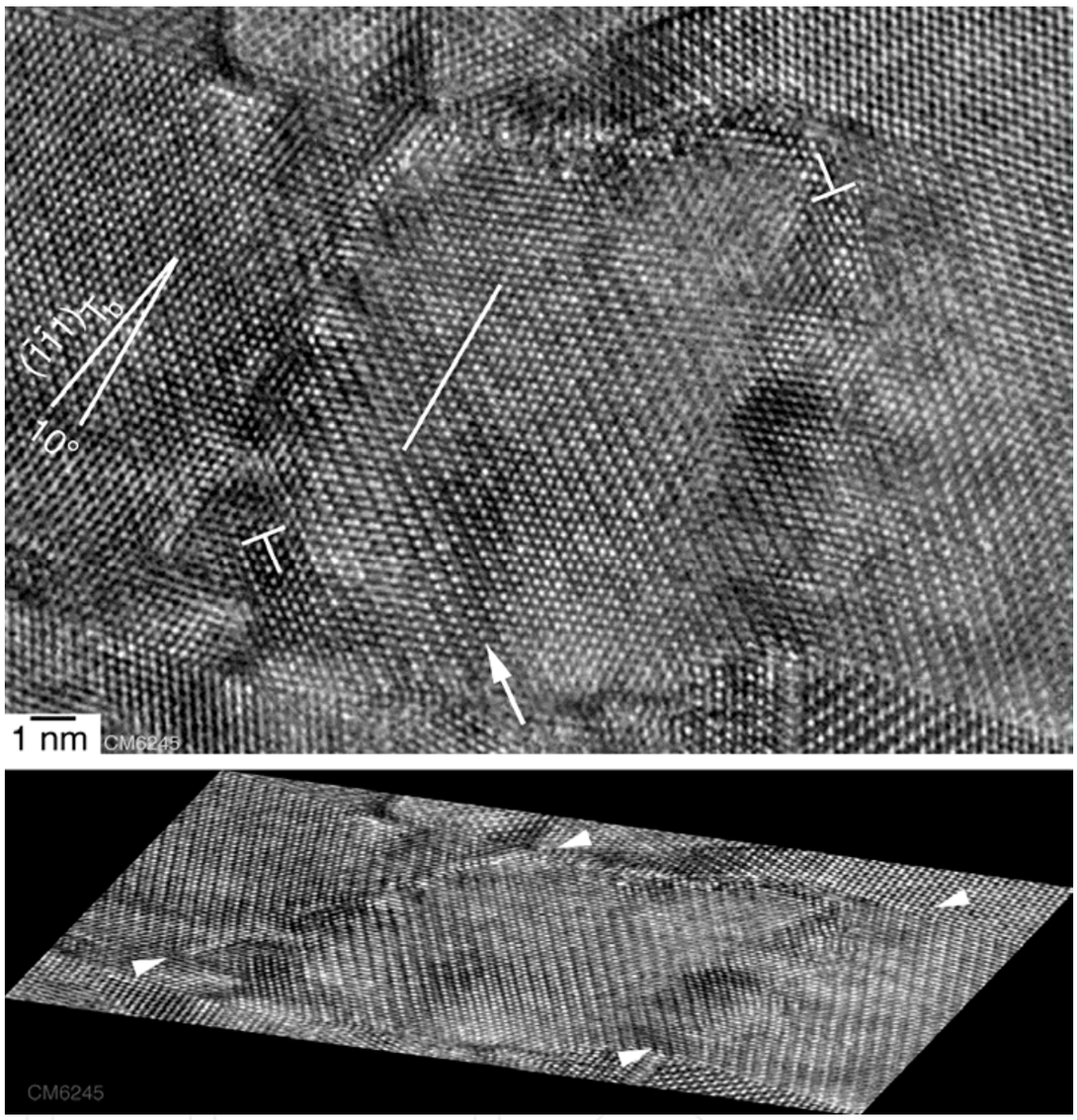

Fig. 10. Structural details of the intersection zone: translation of the twinning shear along the $(\bar{1}\bar{1}1)_{Tb}$ planes by $1/2<10\bar{1}]$ superpartials that become evident by extra $(002)_{Tb}$ planes. Two of the dislocations and their extra half planes are indicated by dislocation symbols. Note the anticlockwise rotation of the intersection zone with respect to the barrier twin by 10°, which is indicated by the traces of the respective $(\bar{1}\bar{1}1)_{Tb}$ planes. The compressed image below shows these features in more detail. Arrowheads mark the dislocation walls on either side of the intersection zone.

are not continuous with those of the barrier twin, but appear displaced along the $(\bar{1}\bar{1}1)_{Tb}$ planes of the barrier twin. This displacement is consistent with glide of $1/2<10\bar{1}]$ or $1/2<01\bar{1}]$ superpartials on $(\bar{1}\bar{1}1)_{Tb}$ planes. These dislocations become manifest by extra $(002)_{Tb}$ planes; a few of these dislocations and the orientation of their extra planes are indicated by dislocation symbols. It is tempting to speculate that these dislocations were

generated under the high stress concentration acting at the corners of the intersection zone. It is worth adding that a shear accommodation by twinning along the $(\overline{1}\overline{1}1)_{Tb}$ planes is not possible because this would require anti-twinning operations. The close distance of these dislocations explains why the lattice of the intersection zone is not congruent with that of the barrier twin, but rotated by about 10° against the barrier twin. The image below is the micrograph compressed along the (002) planes and shows these details more clearly. The observation largely reflects the strong rotation field that was generated by the incident twin. The various dislocation reactions that could be involved in the intersection process probably give rise to dislocation emission; a few of these dislocations are marked with arrows 1 to 3. Twin intersections undoubtedly leave significant internal stresses and dense defect arrangements bordering the intersection zone. Under hot-working conditions these heterogeneities in the deformed state can be the prevalent sites for recrystallization. At elevated temperatures rearrangement of the dislocation walls surrounding the misoriented zone may occur by climb so that the misorientation with respect to the surrounding matrix increases. The intersection zone is transformed into a new grain of low internal energy, growing into deformed material from which it is finally separated by a high-angle boundary. This process is certainly driven by the release of stored energy. Thus, it might be expected that the structural heterogeneities produced by twin intersections act as precursor for recrystallization. Such processes are certainly beneficial for the conversion of the microstructure under hot-working conditions.

3.2 Dynamic recovery

There is good consensus that recovery and recrystallization are competing processes as both are driven by the stored energy of the deformed state. The extent of recovery is generally expected to depend on the stacking fault energy, which, in turn, determines dislocation dissociation. The ordinary dislocations, which mainly carry the deformation in γ(TiAl), have a compact core because dissociation would involve a high-energy complex stacking fault (CSF), which destroys the chemical environment of first neighbours in the fault plane. This compact core structure makes cross slip and climb of the ordinary dislocations relatively easy and is a good precondition for static and dynamic recovery. The most convincing evidence for climb of ordinary dislocations has also been obtained from in situ heating experiments performed inside the TEM [31]. The samples used were pre-deformed at room temperature to a strain of ε=3%; this introduced sufficient dislocations for observation and certainly a small supersaturation of intrinsic point defects. Fig. 11 demonstrates the change of the dislocation fine structure occurring upon heating by a sequence of micrographs. The vacancies produced during room-temperature deformation condense onto screw dislocations, causing them to climb into helices. TEM observations performed after high-temperature deformation have also revealed a remarkable instability of twin structures [31]. Due to these factors, the release of strain energy by recovery is probably relatively easy and can account for the large reduction of the flow stress that has been observed after annealing at moderately high temperatures. Recovery lowers the driving force for recrystallization; thus, a significant amount of prior recovery may retard the recrystallization kinetics. More details about deformation and recovery are provided in [40].

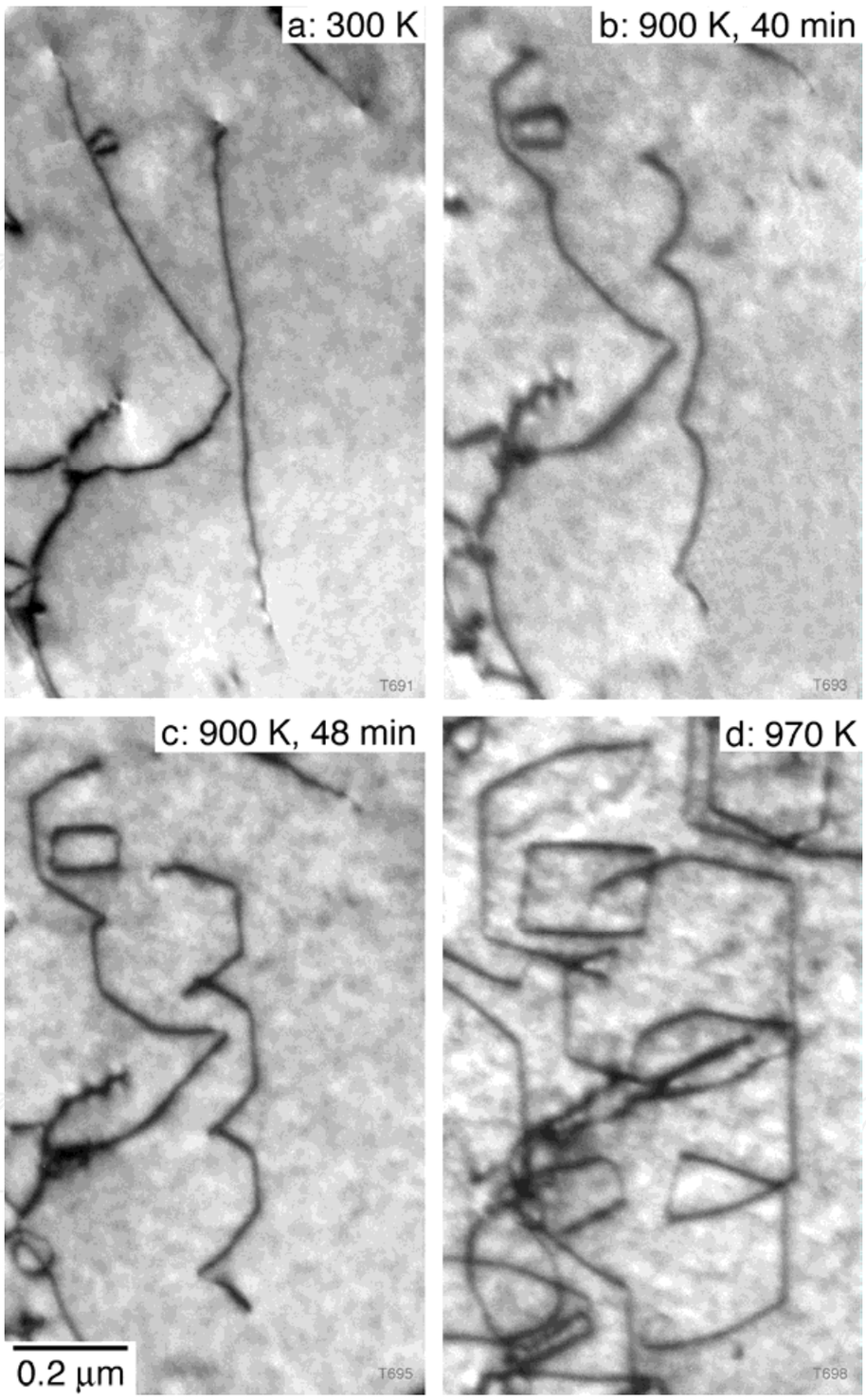

Fig. 11. Climb of ordinary dislocations during in situ heating inside the TEM at an acceleration voltage of 120 kV. Note the formation of a helical dislocation and the growth of prismatic dislocation loops. Cast Ti-48Al-2Cr, pre-deformation at room temperature in compression to ε=3%.

3.3 Dynamic recrystallization

The kinetics of dynamic recrystallization of TiAl alloys depends on several factors; these involve alloy composition, grain size of the starting microstructure, and hot working parameters [41]. The conversion of the coarse-grained lamellar ingot structure is probably the most difficult step in wrought processing. Thus, dynamic recrystallization occurring at this stage will be described as a specific example for TiAl alloys.

There is undisputed evidence that slip transfer through lamellar boundaries is difficult [42]. Plastic strain resulting from a cooperative operation of several deformation modes can be localized between the lamellar boundaries. These facts, combined with the flat plate geometry of the lamellae (Fig. 2), cause a marked plastic anisotropy of lamellar material, which affects the recrystallization behaviour [41]. The recrystallization kinetics is relatively fast if the lamellae orientation is parallel to the deformation axis. Deformation in this orientation apparently involves an element of instability, which is manifested by kinking of the lamellae (Fig. 12) and is reminiscent of buckling of load-carrying structures. In terms of a laminate model [43], the lamellar morphology may be considered as an ensemble of TiAl and Ti_3Al plates. When perfectly aligned with the compression axis, these "columns" are highly stable under compression, as long as the axial load is below a critical value. Above this critical load the equilibrium becomes unstable and the slightest disturbance will cause the structure to buckle. In the lamellar structure an upsetting moment might develop by lateral impinging of the lamellae by dislocation pile-ups or deformation twins. Furthermore, the elastic response of the α_2 and γ phase upon loading is significantly different. Thus, the tendency to instable buckling is expected to increase, if there is an inhomogeneous distribution of α_2 and γ lamellae. The process probably starts with local bending of the lamellae. From the curvature and thickness of the lamellae local strains can be deduced, which are often larger than 10 % and lead to the formation dense dislocation structures and of sub-boundaries (Figs. 13 and 14). Subsequent rotation and coalescence of these sub-grains occurs apparently in such a way that kinking of the lamellae is accomplished. Due to kinking, the lamellae are reoriented with respect to the deformation axis, which may support shearing along the lamellar interfaces. In the regions of highest local bending spheroidization and dissolution of the α_2 phase occur; this suggests that both the non-equilibrium constitution and the local stress provide the driving pressure for the observed phase transformation and recrystallization. All these aspects are manifested in Fig. 15, which shows the initial state of grain nucleation in a kinked α_2 lamella.

Micromechanical modelling [43, 44] has shown that polycrystalline lamellar material deforms very inhomogeneously. Localized stress concentrations have been recognized, which developed within the polycrystal upon straining due to the variations of grain size, shape and orientation. This led the authors to believe that constraints imposed by neighbouring grains are a dominant factor in determining the flow behaviour. Even under compression, very high tensile hydrostatic stresses are generated at the triple points of colony boundaries. There is a strong tendency to develop shear bands, kink bands, lattice rotations, and internal buckling of lamellae. The shear bands consist of extremely fine grains and may traverse the whole work piece, often resulting in gross failure. From a mechanical point of view, buckling failures do not depend on the yield strength of the material but only on the dimensions of the structure and the elastic properties of the material. In lamellar alloys of given lamellar spacing, the tendency to buckling and shear band formation

increases with the axial length of plates. Thus, coarse-grained lamellar alloys seem to be prone to deformation instabilities and shear band formation, which turns out to be one of the prime problems in wrought processing of TiAl alloys.

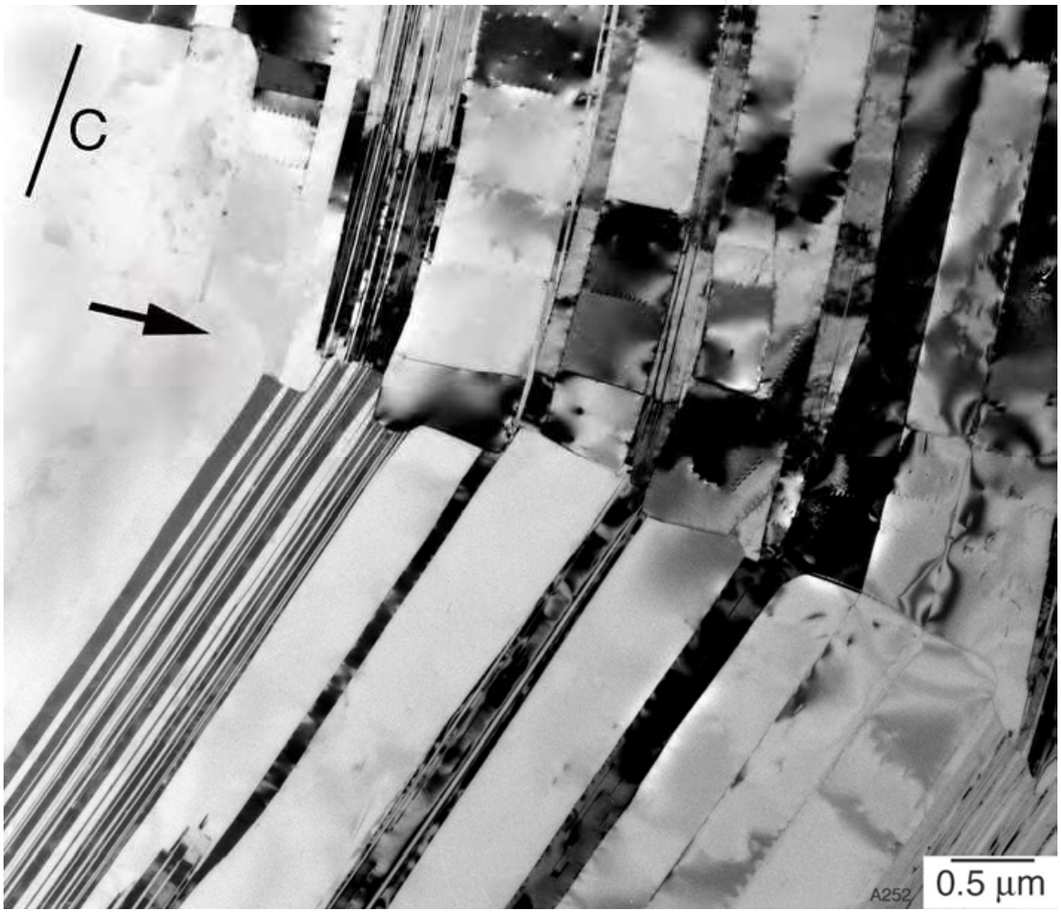

Fig. 12. Kinked lamellae in Ti-47Al-5Nb-0.2B-0.2C. The lamellar ingot material was subject at 1270 °C to a compression stress of σ=(25.4±12.7) MPa fluctuating with 30 Hz. C indicates the orientation of the compression axis, which is parallel to the image plane.

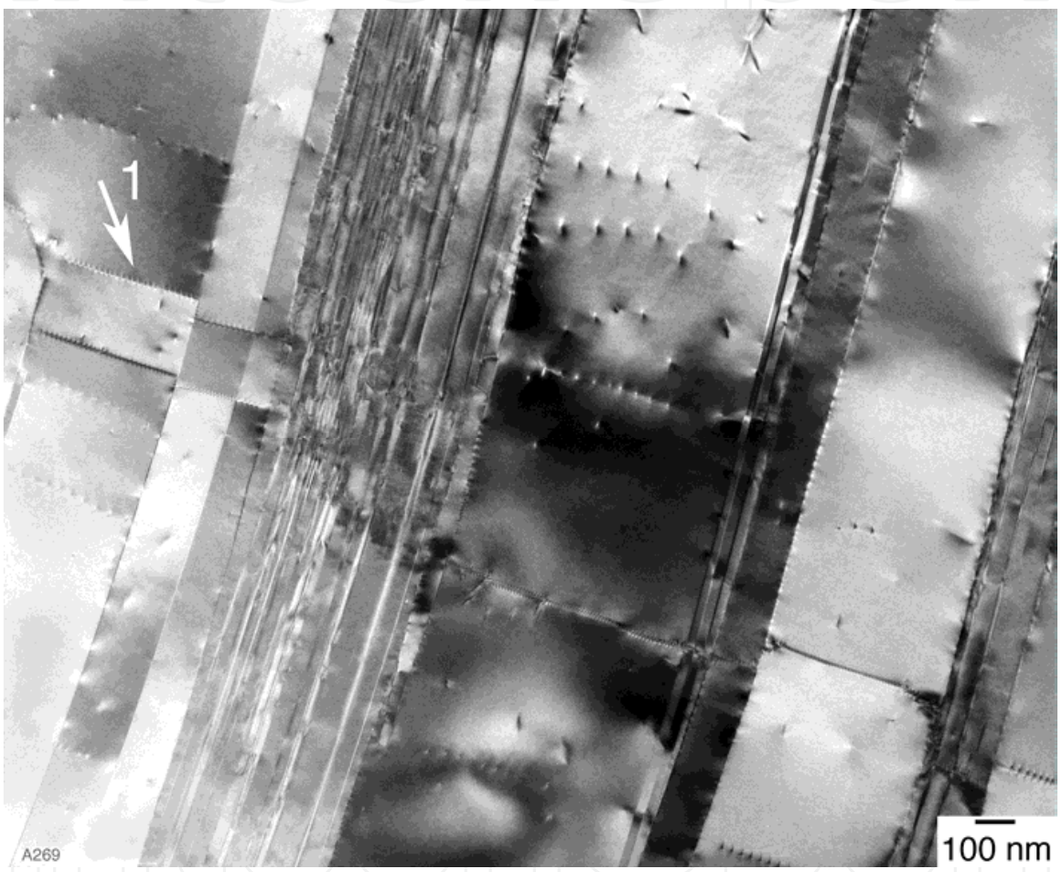

Fig. 13. Sub-boundaries formed at kinked lamellae. Experimental details as for Fig. 12.

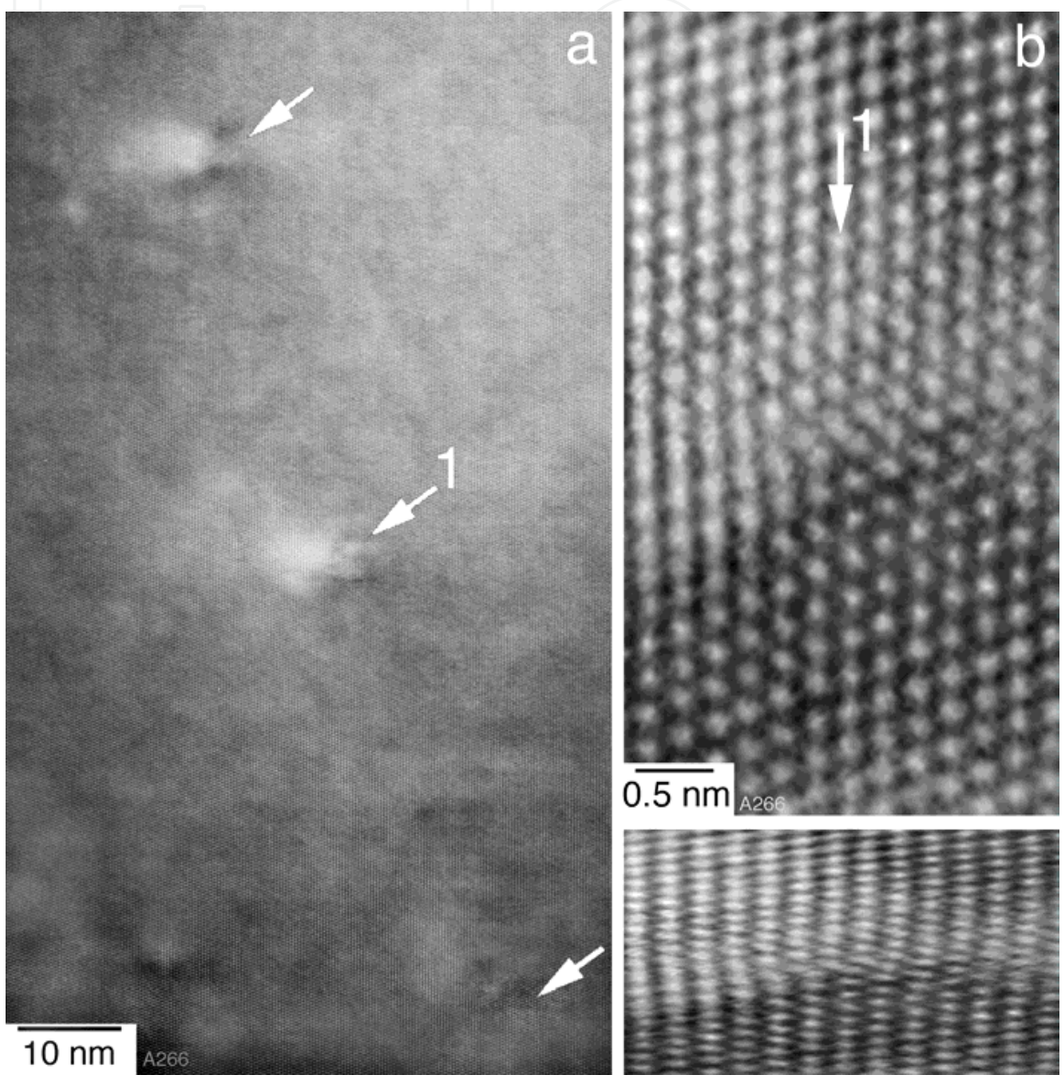

Fig. 14. Atomic structure of a sub-boundary formed at kinked γ lamella; experimental details as for Fig. 12. (a) Mixed ordinary dislocations situated in the sub-boundary (marked with arrow 1 in Fig. 13) and (b) on of the dislocations shown in higher magnification; the compressed image below shows the extra plane of the dislocation more clearly.

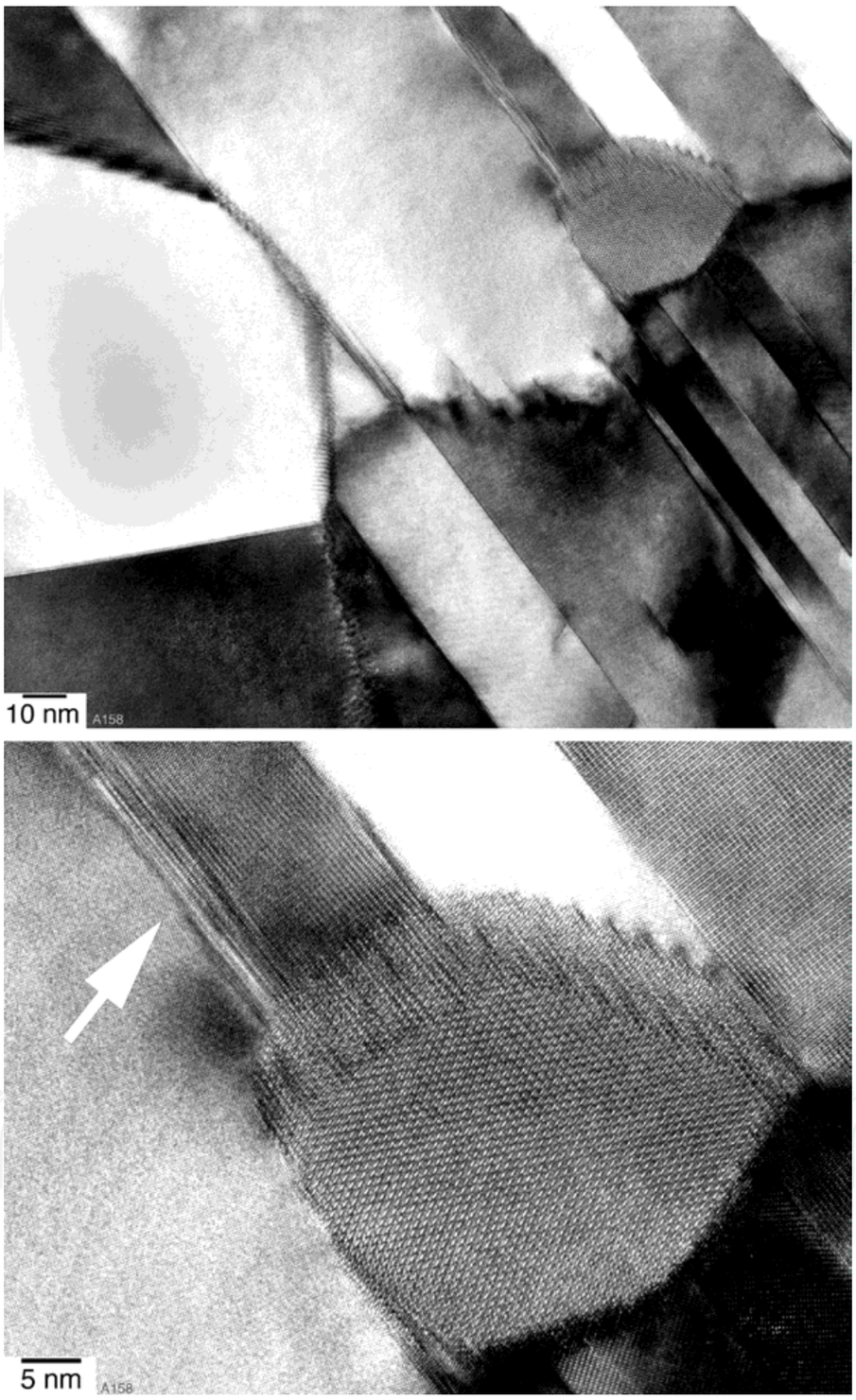

Fig. 15. Initial state of grain nucleation at kinked α_2 lamellae. The image below shows one of the grains in higher magnification. Note the shear processes occurring along the lamellae. Ti-45Al-8Nb-0.2C, sheet material; viewing direction in the transverse direction of the rolling plane.

4. Service-induced phase transformation and recrystallization

4.1 Creep

At temperatures above 650 °C damage of TiAl components may occur due to continuous creep. The relevant mechanisms are numerous and synergistic, depending on the operation conditions; for a review see [45]. Among the various microstructures that can be established in polycrystalline ($\alpha_2+\gamma$) alloys, fully lamellar alloys are most creep resistant. However, numerous investigations have demonstrated that the lamellar microstructure degrades upon creep. This structural instability is a serious problem for long-time service of lamellar alloys. In the following, a few examples of TEM analysis will be presented, which demonstrate the complexity of the processes involved in the degradation of the lamellar morphology. Most of these studies have been performed on samples that had been subject to long-term tensile creep at 700 °C under relatively low stresses of 80 to 140 MPa [46].

When compared with the microstructure of undeformed material, the lamellar interfaces in crept samples were highly imperfect. Figure 16a demonstrates the formation of a high interfacial step in a 60° pseudo twin boundary. The interfacial steps had often grown into broad zones, which extended over about 200 nm perpendicular to the interface; Fig. 16b demonstrates an intermediate stage of this growth process. Multiple-height ledges are commonly observed after phase transformation and growth, and several mechanisms have been proposed to explain the phenomenon [47]. Analogous to these models it is speculated that the large ledges observed in the crept TiAl alloy arise from one-plane steps, which moved under diffusional control along the interfaces and were piled up at misfit dislocations. A misfit dislocation with a Burgers vector component out of the interfacial plane is arrowed in Fig. 16a. Once a sharp pile up is formed, the configuration may rearrange into a tilt configuration with a long-range stress field. This would cause further perfect or Shockley partial dislocations to be incorporated into the ledge and would also explain that in all cases the ledges were associated with misfit dislocations. The detailed atomic structure of the macro ledges is not clear. As can be seen in Figs. 16, there is a variation of the contrast in the ledges with a periodicity of three (111) planes. This is reminiscent of the 9R structure, which is a phase that probably has a slightly higher energy than the $L1_0$ ground state. The formation of the 9R structure is a well-known phenomenon in many f.c.c. metals that exhibit twinning. Singh and Howe [48] have recognized the 9R structure in heavily deformed TiAl. It should be noted, however, that similar three-plane structures have been observed in a massively transformed, but undeformed Ti-48.7Al [49]. In this work the contrast phenomena have been interpreted as arising from overlapping twin related γ variants. Nevertheless, the macro-ledges are a characteristic feature in the microstructure of crept samples and represent at least a highly faulted $L1_0$ structure; the question is only whether there is a periodicity in the fault arrangement. When the macro-ledges grow further, it might be energetically favourable to reconstruct the $L1_0$ structure and to nucleate a new γ grain. Figure 17 probably demonstrates an early stage of such a process. The recrystallized grains usually have a certain orientation relationship with respect to the parent γ lamellae; Fig. 18 indicates that the (001) planes of the recrystallized grain are parallel to the $(1\bar{1}\bar{1})$ planes in the parent lamella γ_1. There is a significant mismatch for this orientation relationship, which is manifested by a high density of ledges and dislocations at the $(001)||(1\bar{1}\bar{1})$ interface. Recrystallization of ordered structures has been investigated in

several studies [50, 51]. There is a drastic reduction in grain boundary mobility, when compared with disordered metals. Recovery of ordered alloys is also complicated by the fact that the ordered state has to be restored. In this respect it is interesting to note that the small grain shown in Fig. 18 is completely ordered giving the impression that the ordering is immediately established after grain nucleation or that nucleation occurred in the ordered state. This might be a consequence of the fine scale of the lamellar microstructure and the heterogeneous grain nucleation at the interfacial ledges. There are certainly crystallographic constraints exerted by the parent lamellae adjacent to the ledges, which may control nucleation and growth. Clearly, the process needs further investigation.

There is a significant body of evidence in the TiAl literature indicating that dissolution of α_2 lamellae occurs during creep [45, 46]. The phase transformation is probably driven by a non-equilibrium constitution. High-temperature creep is expected to promote phase transformation towards equilibrium constitution; thus, dissolution of α_2 and formation of γ occurs [52]. The high-resolution micrograph shown in Fig. 19 supports this reasoning; there is clear evidence that the density of steps at the α_2/γ interfaces is significantly higher than that at the γ/γ interfaces, meaning that the α_2 lamella dissolves, whereas the γ lamellae are relatively stable. The processes eventually end with the formation of new grains (Fig. 20) and a more or less complete conversion of the lamellar morphology into a fine spheroidized microstructure. The $\alpha_2 \rightarrow \gamma$ phase transformation is often associated with local deformation, as suggested by Fig. 21. The micrograph shows two α_2 terminations that are connected by an interface, thus the α_2 lamella is partially dissolved. Two twins were emitted at one of the terminations and a dislocation with a Burgers vector out of the interface is present (Fig. 22). The α_2 terminations have extremely small principal radii of curvature. The elimination of such structural features reduces the surface energy and provides a driving force towards further coarsening. The interface connecting the two α_2 terminations exhibits a fault translation that corresponds to an intrinsic stacking fault. This is indicated by the stacking sequence *ABC B CAB*. The nature of the interface between two phases is determined by their structural relationships. There is a strong tendency for planes and directions with the highest atomic densities to align across the interface. As suggested by Chalmers and Gleiter [53], a better atomic fit at a boundary could result if atoms were moved away from coincident sites by a rigid-body displacement of one grain relative to the other by a constant displacement vector. Atomic modelling performed in this context (for a review see [33]) has shown that the energy of lamellar interfaces could be minimized by a rigid-body translation along the vectors $f_{APB}=1/2<10\bar{1}]_\gamma$, $f_{SISF}=1/6[11\bar{2}]_\gamma$ and $f_{CSF}=1/6[\bar{2}11]_\gamma$. These translations correspond to the formation of an antiphase boundary (APB), a superlattice intrinsic stacking fault (SISF) and a complex stacking fault (CSF), respectively, at the interface. In the present case the translation vector is of type $f_{SISF}=1/6[11\bar{2}]_\gamma$. The observation underlines once again the fine scale of interface processes that may occur during creep of lamellar alloys.

The $\alpha_2 \rightarrow \gamma$ transformation requires a change of both the stacking sequence and the local composition. However, achieving the appropriate composition requires long-range diffusion, which at a creep temperature of 700 °C is very sluggish. Low-temperature diffusion might be supported by the presence of Ti_{Al} antisite defects [6, 32]. In the newly formed γ phase a high density of such defects is certainly formed, in order to accommodate the excess of titanium. Thus, a substantial antistructural disorder occurs, which forms a

percolating substructure. Under such conditions, the antisite defects may significantly contribute to diffusion because antistructural bridges (ASB's) are formed. An elementary bridge event involving one vacancy and one antisite defect consists of two nearest neighbour jumps, which result in a nearest neighbour displacement of two atoms of the same species. For the $\alpha_2 \rightarrow \gamma$ transformation the so-called ASB-2 mechanism [32] might be relevant, which requires only low migration energy. Diffusion may also be supported by the mismatch structures present at the interfaces. Dislocations and ledges represent regions where the deviation from the ideal crystalline structure is concentrated. These are paths of easy diffusion, which can effectively support the exchange of Ti and Al atoms. One may expect all these processes to be thermally activated und supported by superimposed external stresses. In this respect, the coherency stresses present at the interfaces are certainly significant because they are comparable to or even higher than the shear stresses applied during creep tests and are often associated with mismatch structures. Thus, given a non-equilibrium constitution, it is understandable that drop in the α_2 volume content also occurs, when a lamellar alloy is subject to the same temperature/time profile without externally applied stress [54].

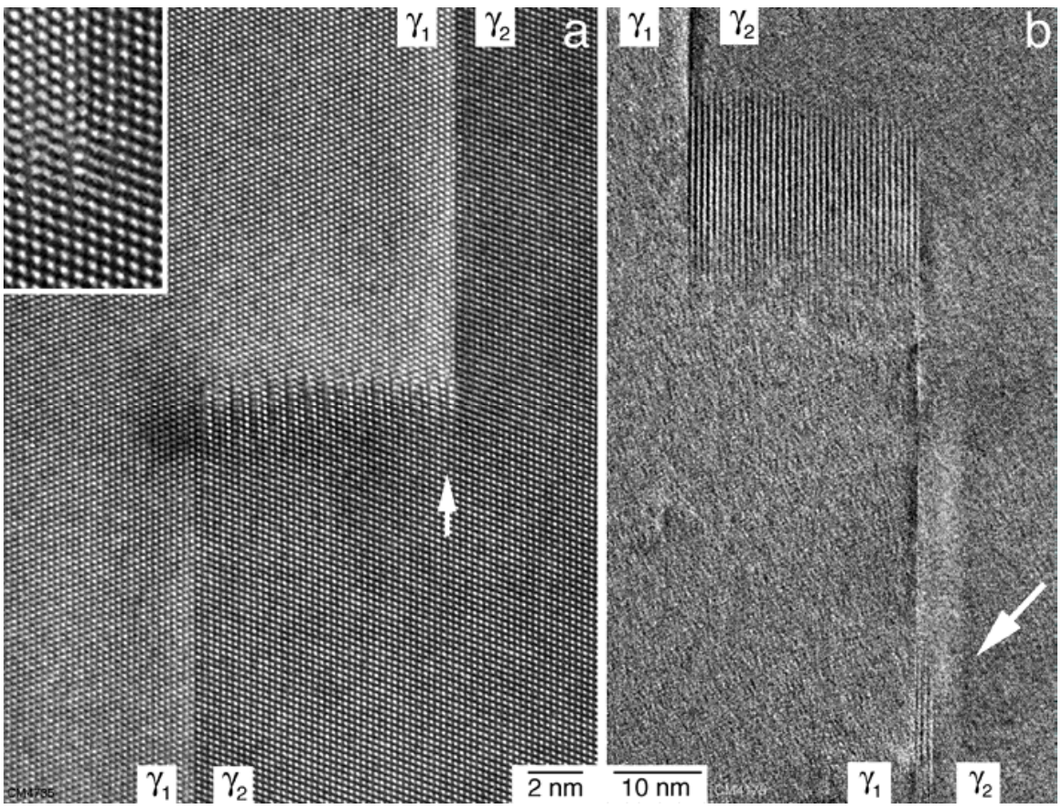

Fig. 16. Degradation of the lamellar structure in Ti-48Al-2Cr under long-term creep at T=700 °C, σ_a=140 MPa, for t=5988 hours to strain ε=0.69 %. (a) Formation of an interfacial step in a 60° pseudo twin boundary. Note the interfacial dislocation (arrowed) that is manifested by an additional {111} plane. (b) A macro-ledge present in a 60° pseudo twin boundary.

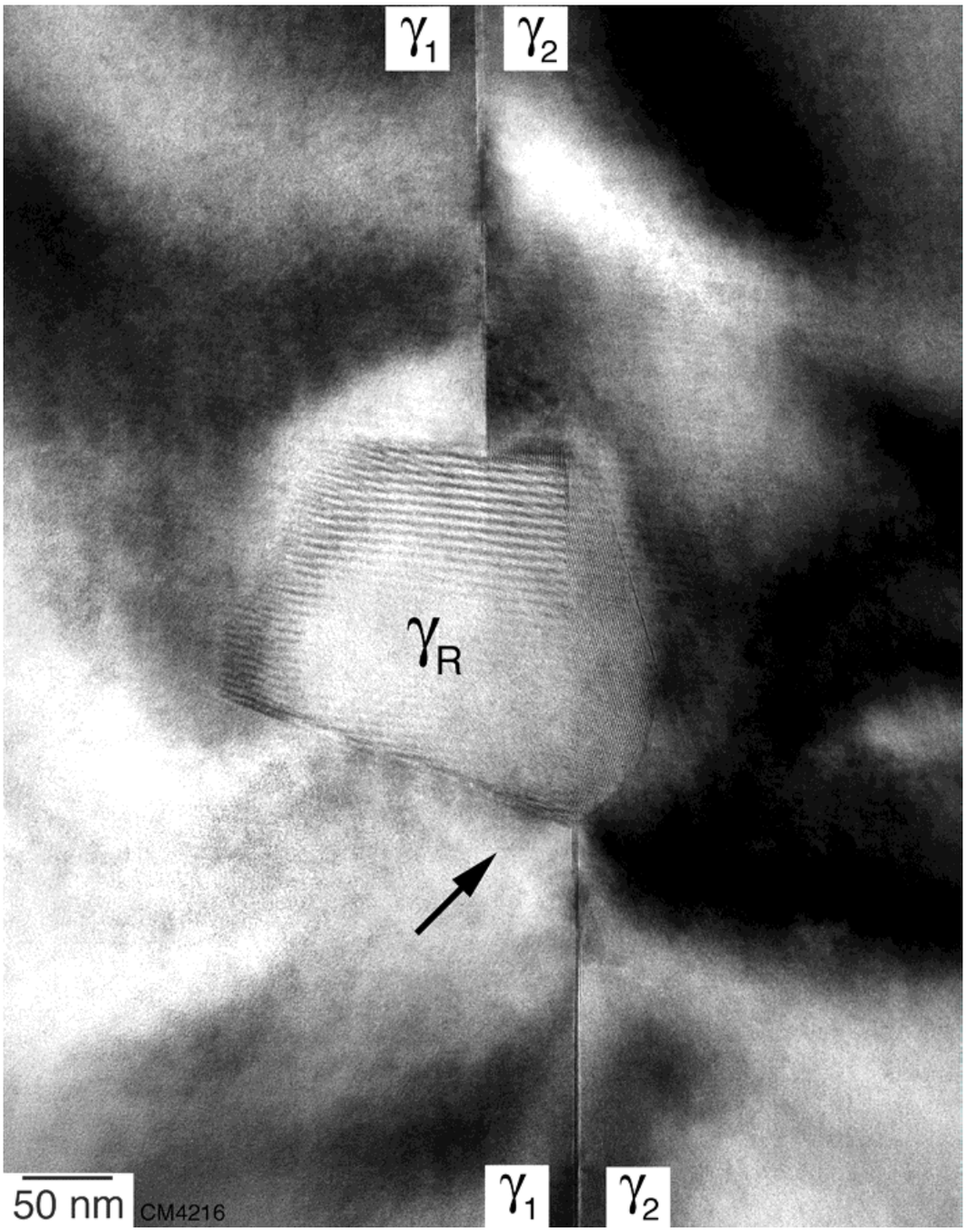

Fig. 17. Recrystallized grain γ_R formed at a ledge in a lamellar interface joining the gamma variants γ_1 and γ_2 with a pseudo twin orientation relationship. Note the step in the interface and the ordered state of the recrystallized grain. Experimental details as for Fig. 16.

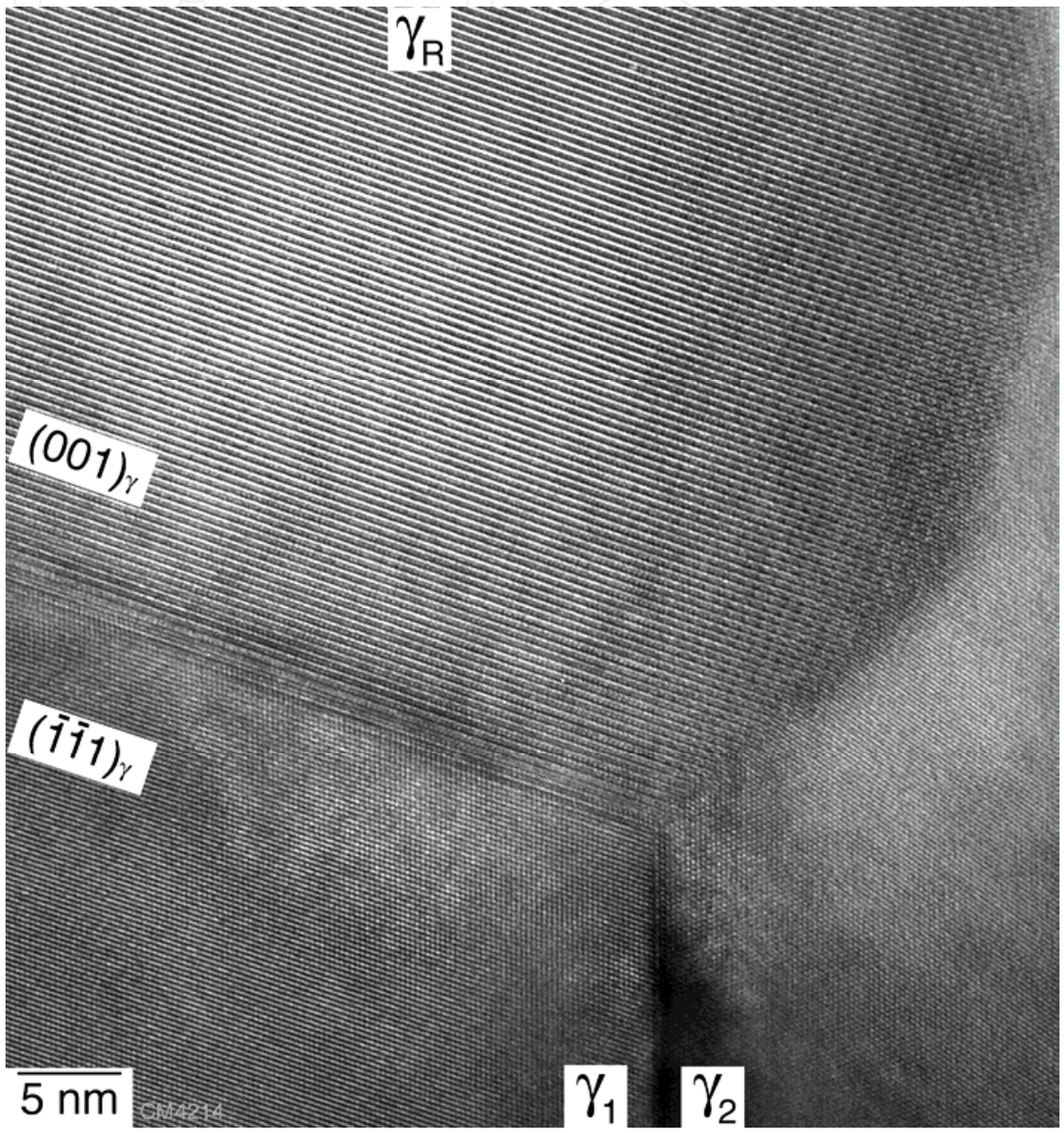

Fig. 18. Higher magnification of the boundary triple-point marked in Fig. 17. Note the orientation relationship (001)||(111) between the recrystallized grain γ_R and lamella γ_1.

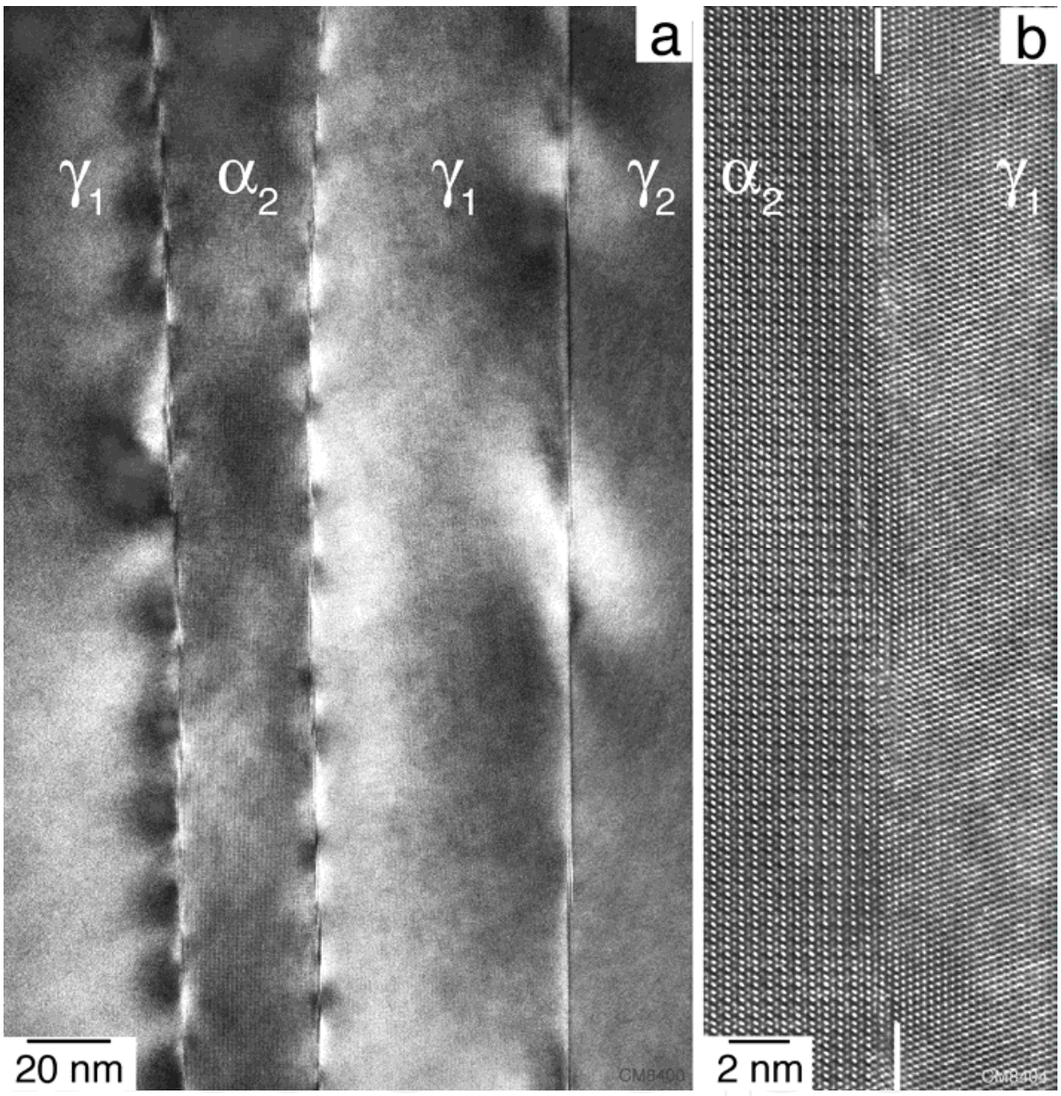

Fig. 19. Initial stage of the $\alpha_2 \rightarrow \gamma$ phase transformation in the lamellar structure of a Ti-48Al-2Cr alloy occurring during long-term creep at T=700 °C, σ_a=110 MPa, t=13400 hours to strain ε=0.46 %. (a) Low-magnification high-resolution image of the lamellar structure. Note the significantly higher density of steps at the α_2/γ interfaces, which indicates dissolution of α_2 phase. (b) Atomic structure of one of the α_2/γ interfaces demonstrating its stepped character.

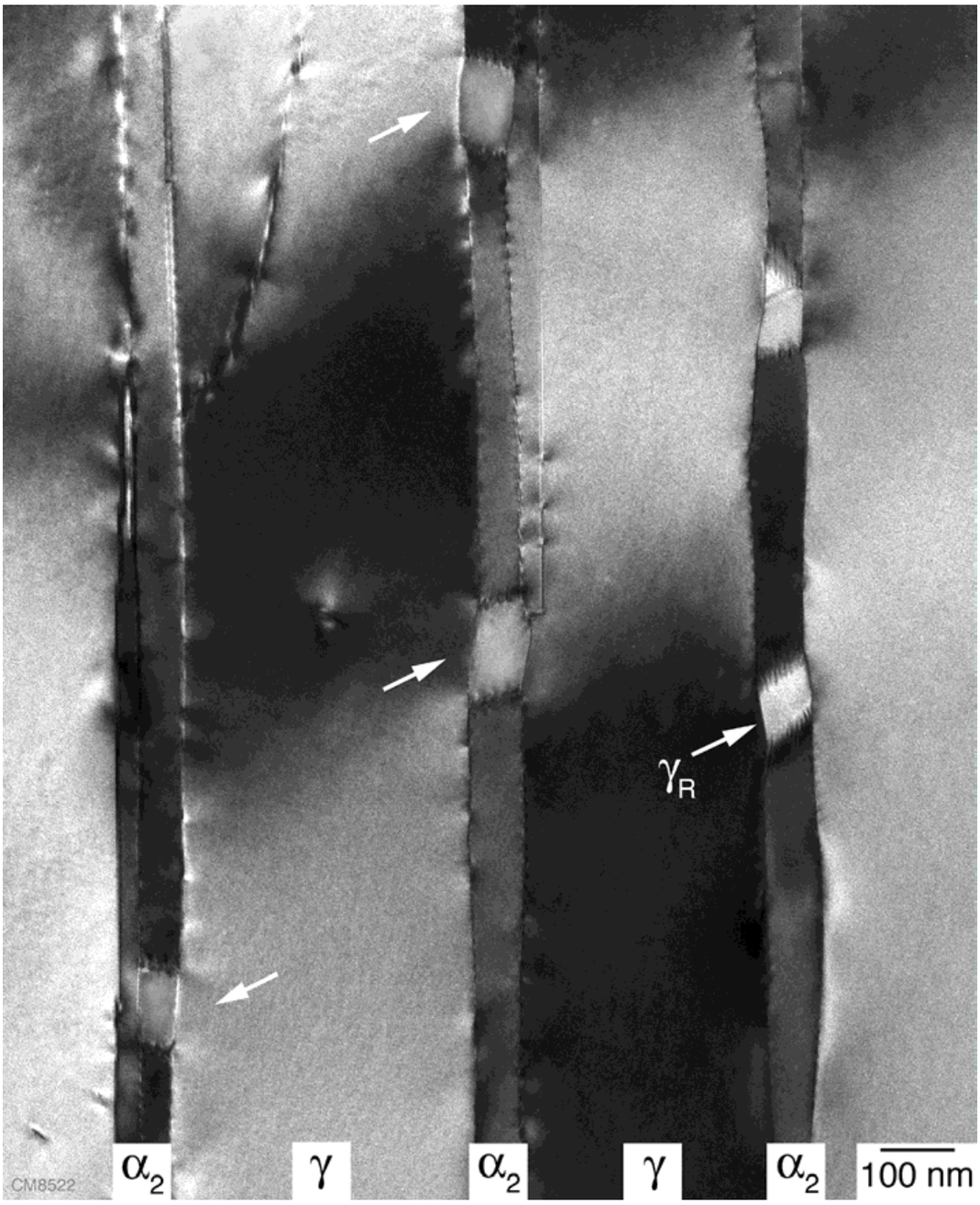

Fig. 20. Spheroidization of α_2 lamellae due to the formation of γ grains (arrowed, designated as γ_R). Experimental details as for Fig. 19.

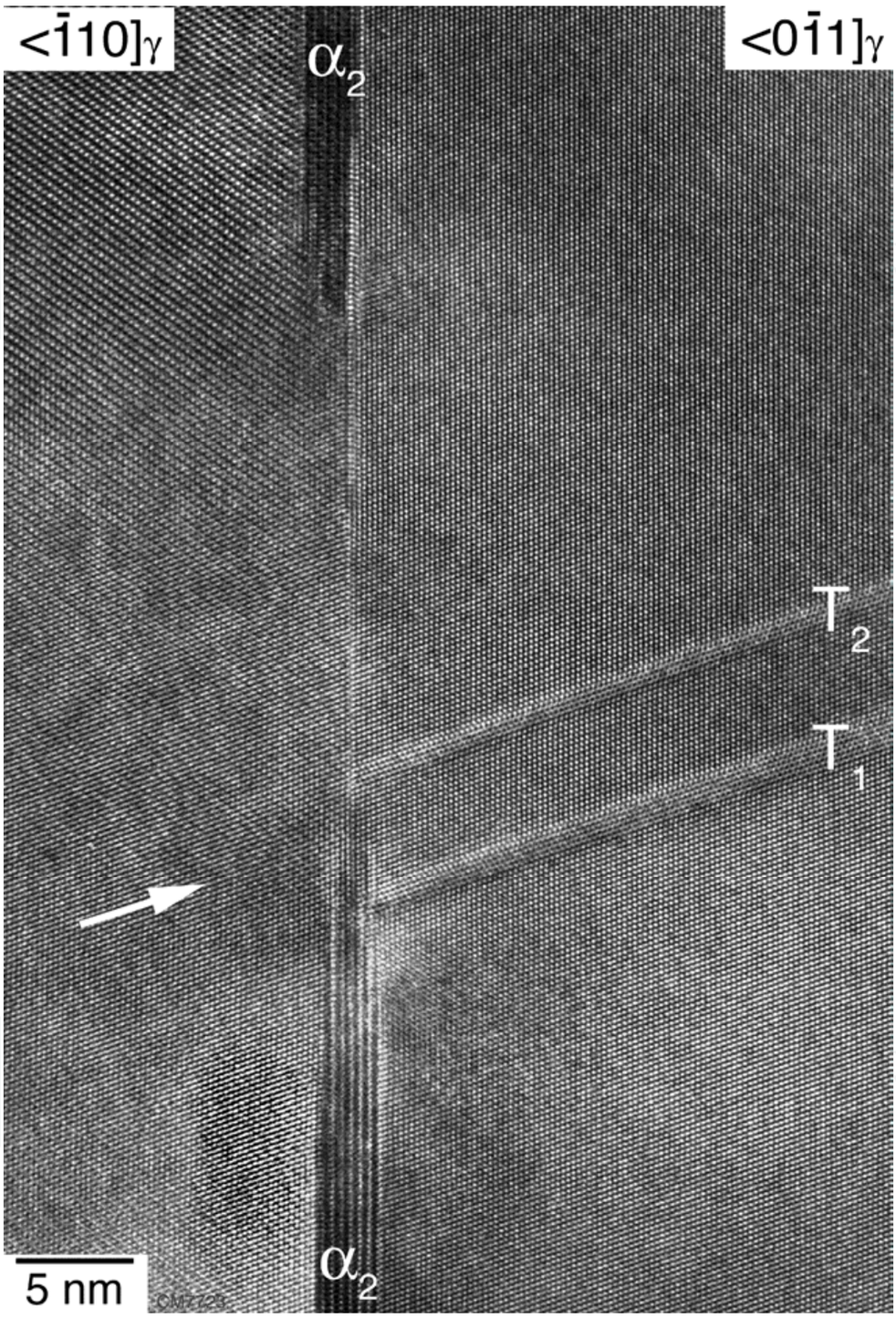

Fig. 21. A partially dissolved α_2 lamella in Ti-46.5Al-4(Cr, Nb, Ta, B) embedded in γ phase. Creep deformation at T=700 °C, σ_a=200 MPa to strain ε=1.35 %. Note the two α_2 terminations that are connected by an interface and the emissions of two twins T_1 and T_2 at one of the terminations. The stacking sequence indicates a rigid body translation of the adjacent γ lamellae.

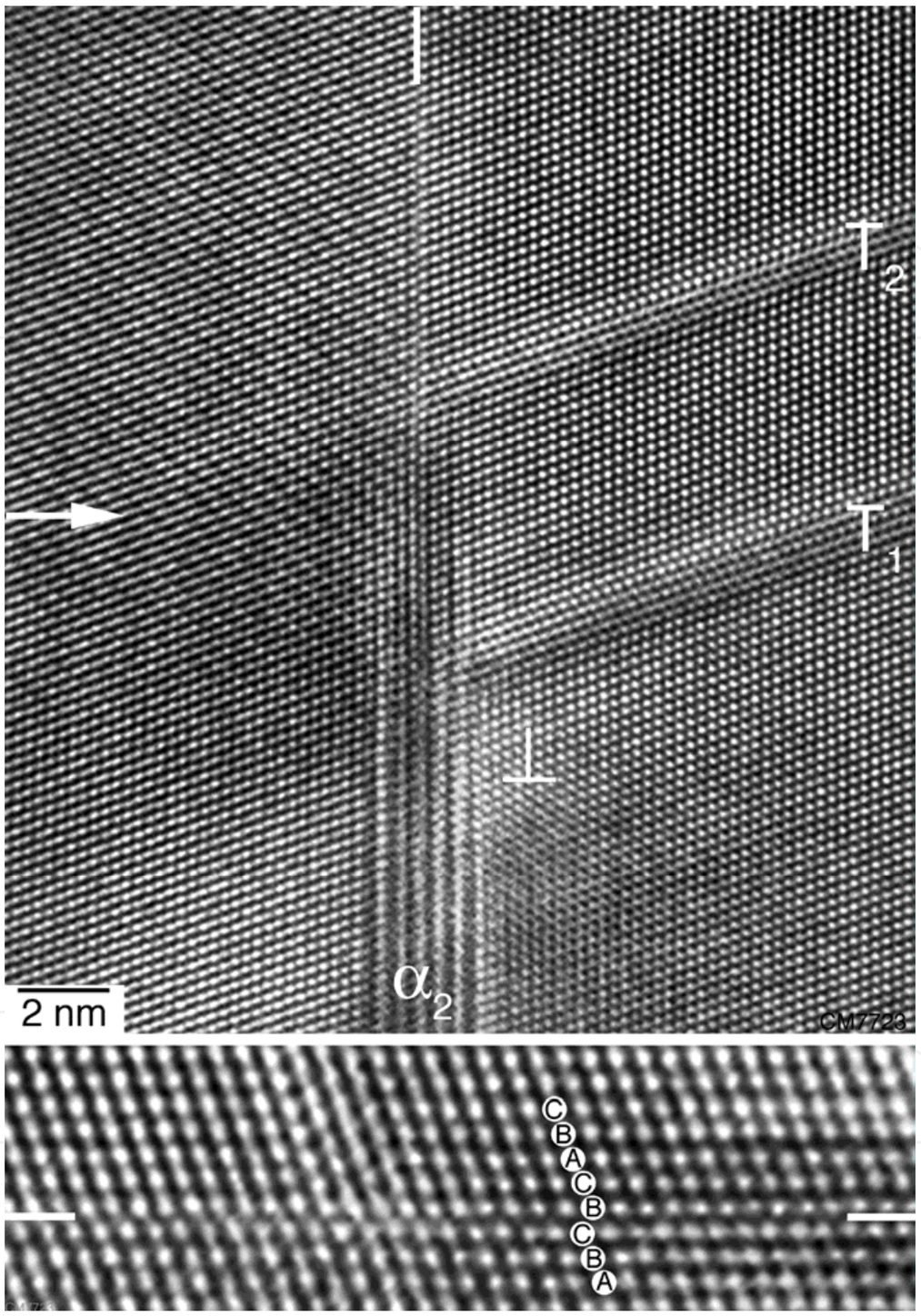

Fig. 22. Higher magnification of the area marked in Fig. 21 showing deformation activity in the vicinity one of the α_2 terminations. Two mechanical twins and a dislocation with a Burgers vector out of the interface plane (marked by symbol) are present. The lower image shows the stacking sequence across the interface (parallel to the arrow) that connects the two α_2 terminations. The stacking sequence indicates the presence of a fault translation.

4.2 Fatigue

By far, the most anticipated engineering applications of TiAl alloys involve components that are subjected to fluctuating or cyclic loading. The capability of TiAl alloys to sustain such loading conditions is inherently limited by the plastic anisotropy at the dislocation level and the lack of independent slip and twinning systems that can operate under reversed plastic straining. Low-cycle fatigue (LCF) is a progressive failure phenomenon brought about by cyclic strains that extend into the plastic range. Thus, the LCF life is largely determined by the amount of inelastic strain in each cycle. While the macroscopic LCF phenomena are well characterized [55], it is only recently that information about the structural degradation occurring upon fatigue has been obtained [56]. A few examples for these processes will be demonstrated in this section.

The fatigue study was performed on an extruded Ti-45Al-8Nb-0.2C alloy (TNB-V2), which contains a significant amount of β/B2 phase and an orthorhombic phase with B19 structure. TEM examination performed after room temperature fatigue has shown that the B19 structure transforms into γ phase. The phase transformation occurs in such a way that extremely fine shear bands are formed (Fig. 23). The result is a lamellar morphology that is comprised of extremely fine γ lamellae adjacent to B19 phase (Fig. 23b). A general observation is that two different γ variants are usually generated adjacent to the B19 phase, as seen for almost all the γ lamellae in Fig. 23b. If, for example, the stacking sequence of the $\{111\}_\gamma$ planes of the variant γ_1 is labelled *ABC*, that of variant γ_2 is *CBA*. This inversion of the stacking sequence is thought to induce strain fields of opposite signs, which eventually reduces the total strain energy. It might be speculated that such a combination of shear processes makes the transformation easier. The transformation often starts at grain boundaries and proceeds through the formation of ledges via distinct atomic shuffle displacements; these details are shown in Fig. 24. It should be noted that the B19→γ transformation has been observed at all the fatigue test temperatures investigated. Due to the difference in lattice constants between the γ and B19 phases the transformation may accommodate local strains and is thus expected to serve as a toughening mechanism. Nevertheless, the life of TiAl testpieces under low cycle fatigue with plastic cyclic strain amplitudes of a few tenth of a percent is limited to a several hundred cycles.

5. Diffusion bonding

Solid-state diffusion bonding provides a means of joining TiAl alloys without melting of the base materials. The principal diffusion bonding parameters, temperature and stress, depend on yield strength, work hardening behaviour and creep resistance of the mating alloy coupons. The bonding conditions should be chosen so that coalescence of contacting surfaces is produced by asperity deformation, but without gross deformation of the component. The effects of bonding temperature and bonding stress are synergistic; at higher temperature less stress is required and vice versa. For more details see [57].

During diffusion bonding of (α_2+γ) alloys a three layer process zone is typically developed that involves a fine grained layer of α_2 phase at the former contact plane of the diffusion couple, a region made up of relatively large recrystallized grains, followed by a region of deformed bulk material (Fig. 25). The bond layer consists of fine stress free grains (Fig. 26), which were identified by EDX and EBSD analysis as α_2 phase. It is well documented in the

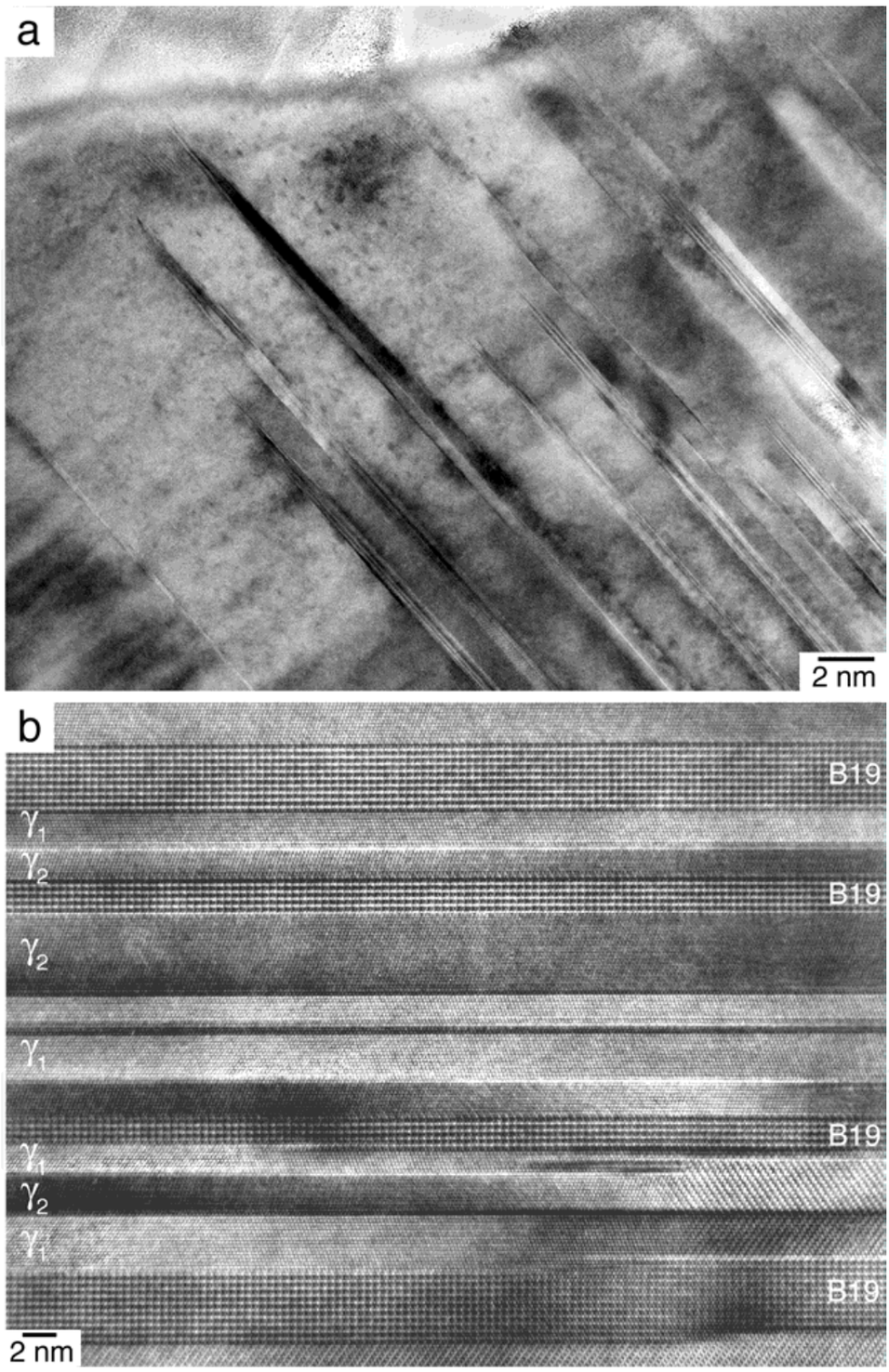

Fig. 23. Phase transformation B19→γ during low cycle fatigue at T=550 °C, $\Delta\varepsilon_t/2=\pm0.7$ %, $N_f=452$; nearly lamellar Ti-45Al-8Nb-0.2C. (a) Low-magnification high-resolution TEM micrograph showing fine γ lamellae produced in the B19 phase. (b) Lamellar morphology consisting of fine γ lamellae adjacent to B19 phase.

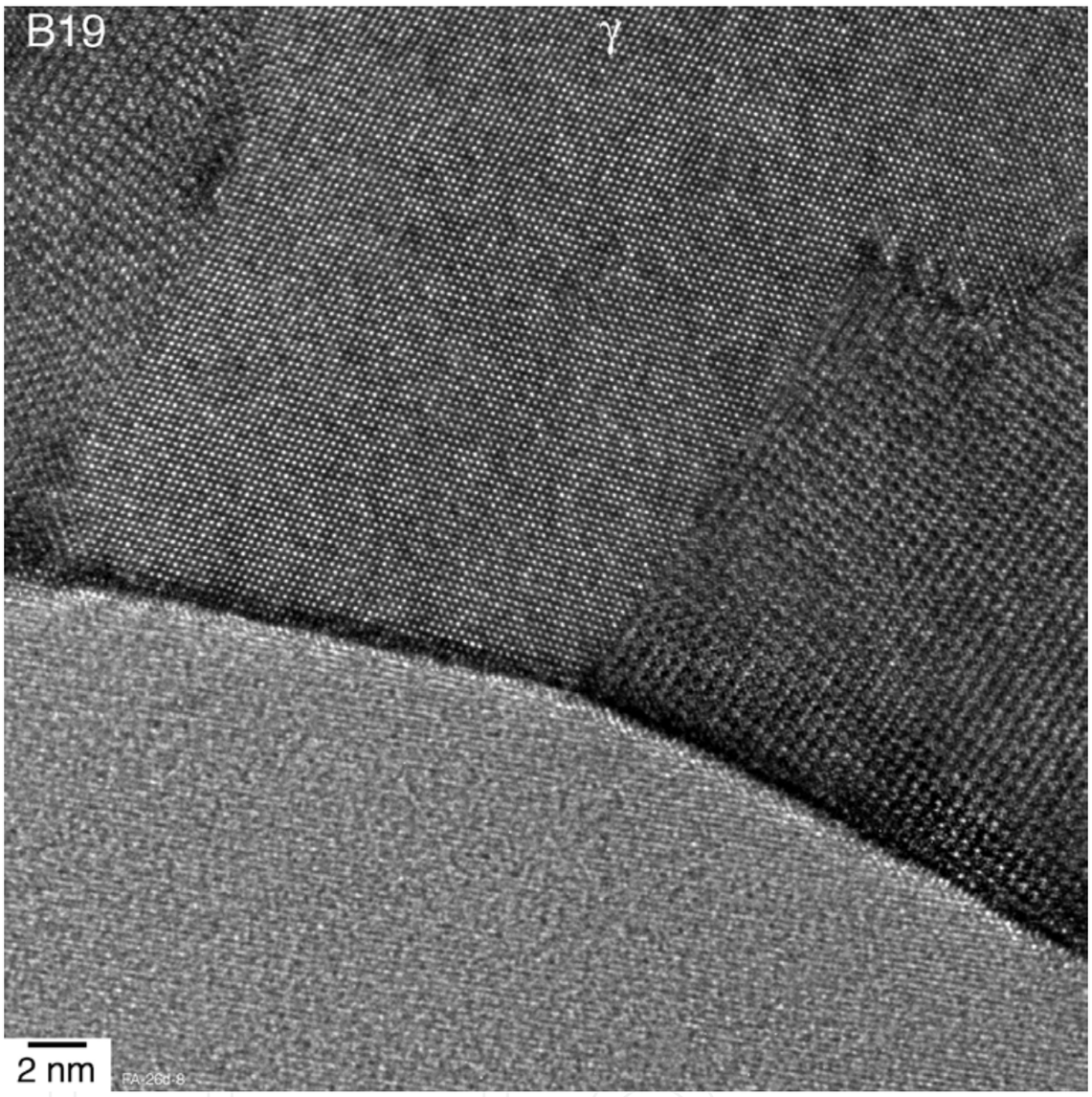

Fig. 24. Transformation B19→γ near to a grain boundary. Nearly lamellar Ti-45Al-8Nb-0.2C, sample fatigued at 25 °C to failure after N=641 cycles with R=-1 and a total strain amplitude $\Delta\varepsilon_t/2$=0.7 %.

literature [58] that a very small amount of oxygen can stabilize the α_2 phase. This finding is consistent with an early investigation of Godfrey et al. [59] performed on diffusion bonded Ti-48Al-2Mn-2Nb. Orientation analysis performed on the α_2 grains has shown that most of the newly formed α_2 grains have an orientation that is suitable for prismatic glide. This data could reflect the well-known plastic anisotropy of the α_2 phase, according to which the activation of prismatic slip along $1/3\langle 11\bar{2}0\rangle\{10\bar{1}0\}$ is by far easiest (Sect. 3.1). It might be speculated that nucleation and growth of new α_2 grains are controlled by the deformation constraints operating during bonding in that the preferred grain orientation ensures strain accommodation on the most favourably slip system.

The α_2 phase at the bond layer is formed at the expense of the Ti content of the adjacent regions, which needs long-range diffusion. The Ti transport could be supported by the anti-structural disorder, as already mentioned in Sect. 4.1. Furthermore, Ti transport could be accomplished by diffusion along the various internal boundaries present in the fine-grained materials. In this respect the lamellar interfaces are probably important because the deviation from the ideal crystal structure occurs and dense arrangements of misfit dislocations are present. Due to the transport processes described, the Ti content of the pre-existing α_2 and β phases situated next to the bonding layer gradually decreases and eventually falls below the critical composition required for their existence; eventually, these phases transform into γ(TiAl). The effect is most pronounced in lamellar colonies that are in contact with the bonding line, presumably because pipe diffusion along the lamellar interfaces is significant. A common observation supporting this mechanism is that the newly formed α_2 grains are connected with pre-existing α_2 lamellae, which in a sense feed the chemically driven generation of α_2 phase at the bonding layer. All in all, the process zone of diffusion bonded TiAl couples reflects the combined influences of chemical driving pressure due to the oxygen contamination at the bonding surfaces and dynamic recrystallization induced by asperity surface deformation.

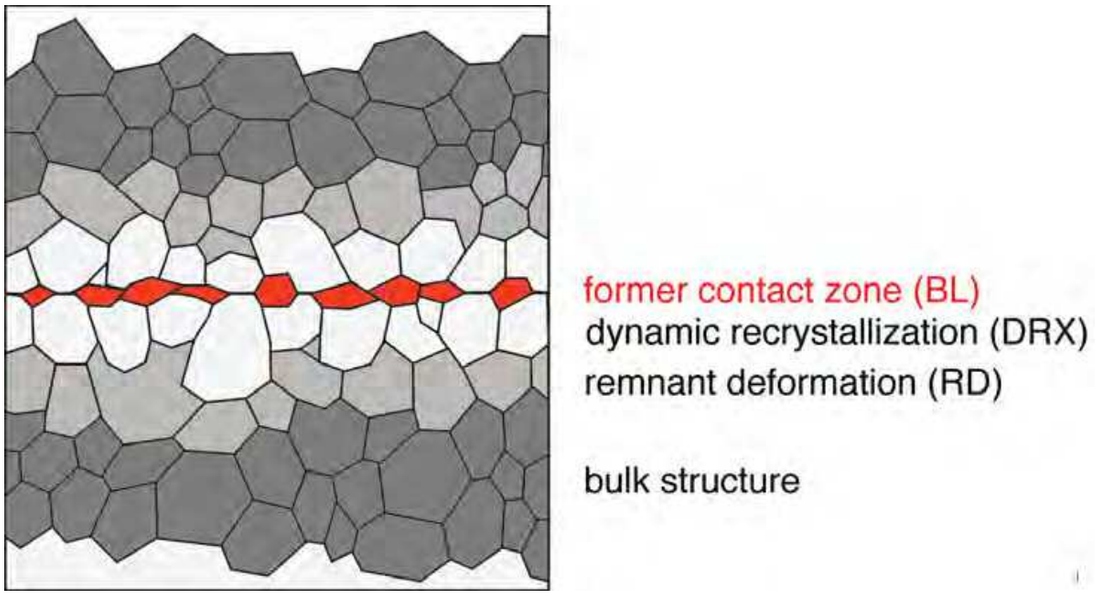

Fig. 25. Schematic illustration of the process zone observed after diffusion bonding at relatively low stresses. BL - fine grained bond layer at the former contact plane of the diffusion couple, DRX - region consisting of relatively large recrystallized grains, RD - initial bulk material but with remnant plastic deformation.

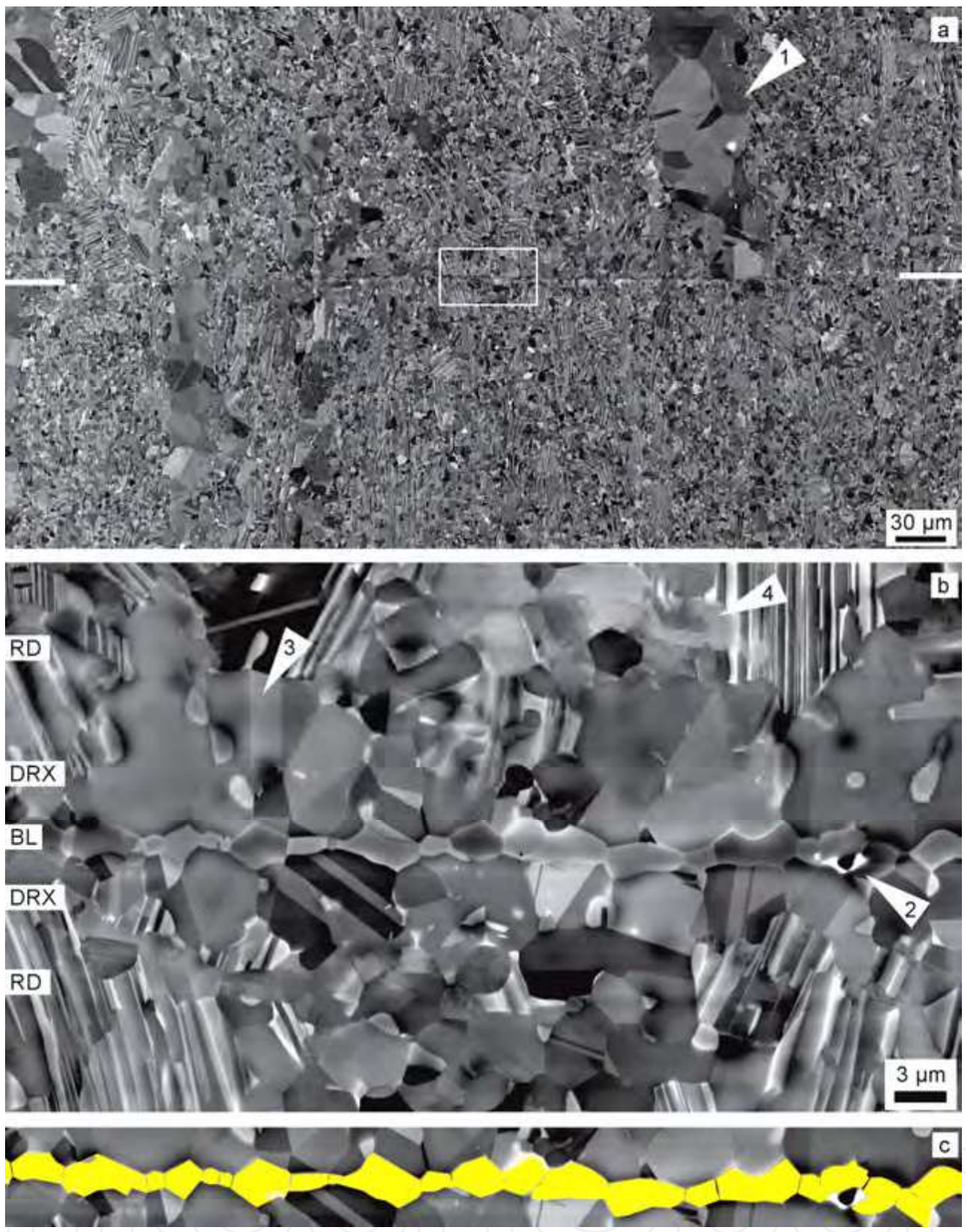

Fig. 26. Cross section of a bond in Ti-46.5Al formed at T= 1273K, σ=20 MPa and t=2h. Scanning electron micrographs taken in the backscattered mode. (a) Low magnification image showing the gross structure of the bond; the horizontally oriented bonding layer is marked by white bars. Note the inhomogeneity of the starting material that is manifested by a banded structure parallel to the extrusion direction (vertical in the micrograph) involving remnant lamellae, fine-grained regions and large γ grains (arrow 1). (b) Higher magnification of the area boxed in (a) showing the bonding layer BL, the recrystallized region DRX and the region with remnant deformation RD in more detail. Note the pore in the bonding layer (arrow 2) and the annealing twins in the γ grains of the DRX region (arrows 3 and 4). (c) Bonding layer consisting of fine-grained α_2 phase as identified by EBSD and EDX analysis [57].

6. Shot peening

Shot peening is a cold working process in which the surface of a component is blasted with small spherical media called shot. A compressive layer is formed by a combination of subsurface compression developed at the Hertzian impression combined with lateral displacement of the surface material around each of the dimples formed. Since fatigue cracks will not initiate nor propagate in compressively stressed regions, shot peening can greatly enhance fatigue life.

In TiAl alloys shot peening produces a heavily deformed surface layer with a thickness of 10 μm to 80 μm depending on the microstructure and yield stress of the substrate alloy [60]. Deformation is characterized by intensive glide and mechanical twinning, involving all potential slip systems available in the major phases $\alpha_2(Ti_3Al)$ and $\gamma(TiAl)$, not only the easy ones. On the mesoscopic scale, buckling and kinking of the lamellae manifest deformation. TEM observations have revealed a remarkable conversion of the microstructure involving dynamic recrystallization and $\alpha_2 \rightarrow \gamma$ phase transformation. The phase transformation starts with a splitting of α_2 lamellae at positions of strong bending or kinking, where the elastic stresses are highest. Another prominent damage mechanism is amorphisation. As shown in Fig. 27a, nano-crystalline grains are embedded in an almost featureless amorphous phase; Fig. 27b demonstrates the gradual loss of crystallinity towards to the adjacent amorphous phase. There seems to be a significant mismatch between the crystalline and amorphous phases, which is indicated by a systematic array of like dislocations (Fig. 28). From the dislocation separation distance it may be concluded that the mismatch is at least 2 % to 5 %.

The observation of an amorphous phase is surprising. However, there are a few arguments that make its existence plausible. Firstly, in the surface layer the material undergoes severe plastic deformation. This introduces various defects, raises the free energy, and creates fresh surfaces due to the formation of slip steps and localized cracking. Secondly, there is certainly a substantial pick up of nitrogen, oxygen, and perhaps hydrogen because the shot peening was performed in air. Thus, several metastable nitride, oxide and hydride phases can be formed. The presence of these interstitial elements in the α_2 and γ phases may favour their amorphisation. Unfortunately, the nature of the crystalline grains embedded into the amorphous phase could not be determined, but it might be speculated that they are oxide, nitride or hydride phases. The formation of one of these crystalline surface phases could be an intermediate state before amorphisation eventually starts. This is suggested by two observations. The crystalline surface phase contains a high density of dislocations, which are often arranged in dipole or multipole configurations. The compressed image reveals significant bending of the lattice planes, which suggests high internal stresses. Another remarkable feature of the crystalline surface phase is antiphase boundaries (APB), as seen in Fig. 29. The APB's provide a local loss of order and are often associated with adjacent amorphous phase. Thus, it is speculated that the formation of APB's represents the initial stage of amorphisation.

Taken together, theses factors apparently make the crystalline surface phase prone to further structural changes, which could be directly observed in the electron microscope. Figure 30 demonstrates the transformation of the crystalline phase by a couple of micrographs. The slurry contrast in the micrograph on the left hand side indicates that the structure was about to transform into the structure shown on the right hand side. The observed conversion of the structure usually involved a very small volume of several ten nanometres and often occurred within a few ten seconds.

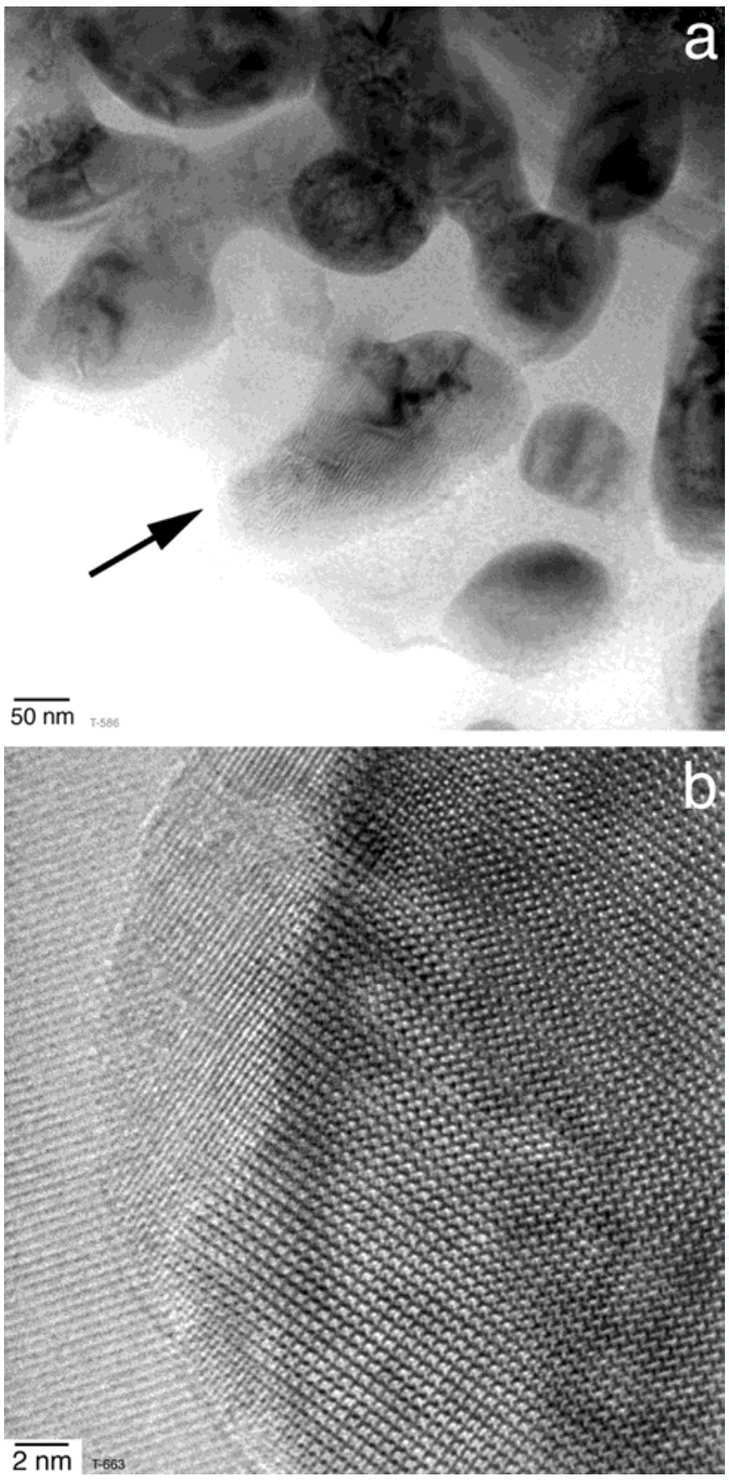

Fig. 27. Partial amorphisation in the shot peened surface layer. Lamellar Ti-45Al-10Nb, shot peened at room temperature with an Almen intensity of 0.4 mm N. (a) Crystalline grains embedded in amorphous phase. (b) Gradual loss of crystallinity of a grain adjacent to the amorphous phase.

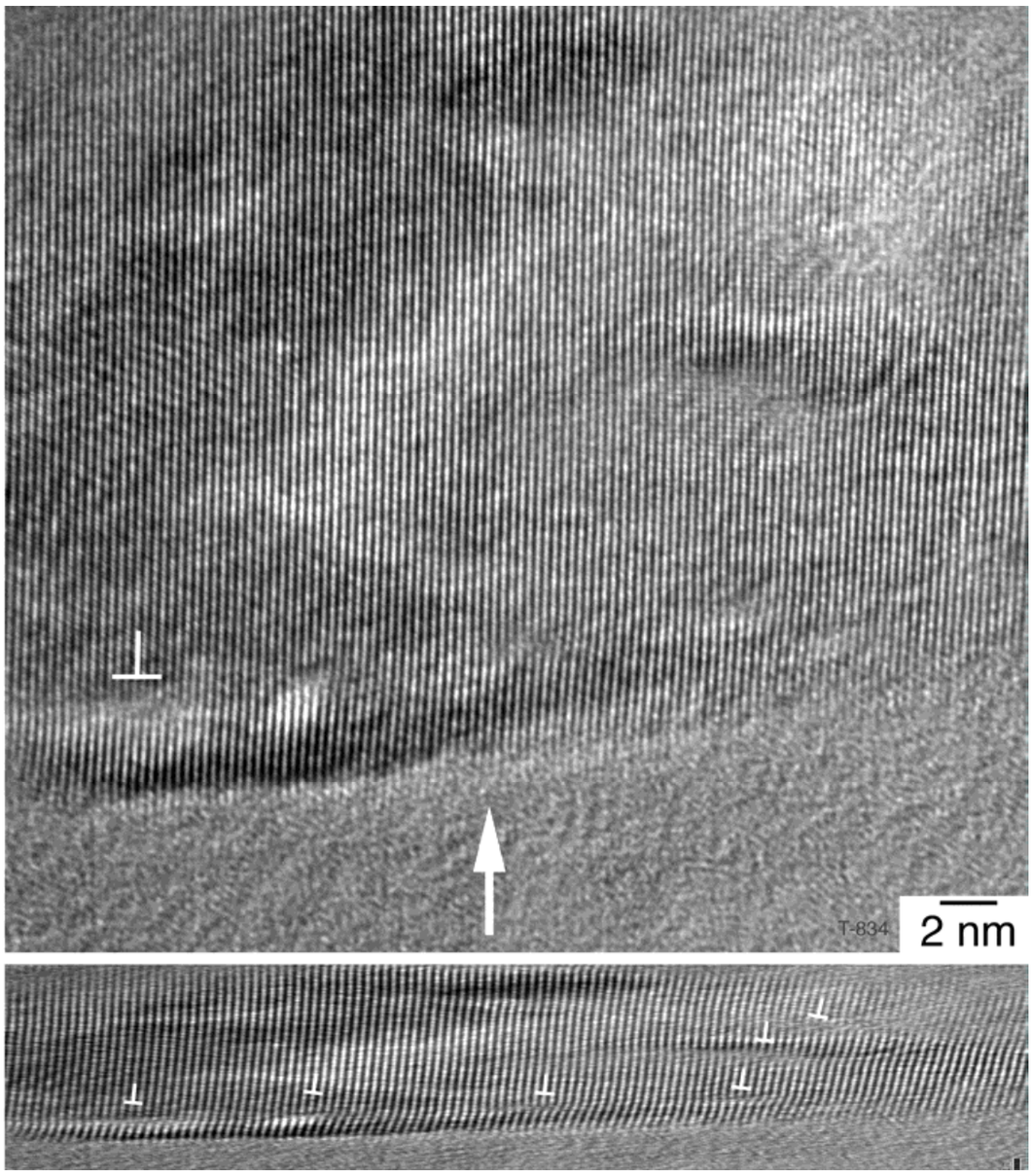

Fig. 28. Misfit between the amorphous and crystalline surface phases produced by shot peening. Note the arrangement of like dislocations at the interface. The compressed image below shows these details more clearly. Experimental conditions as for Fig. 27.

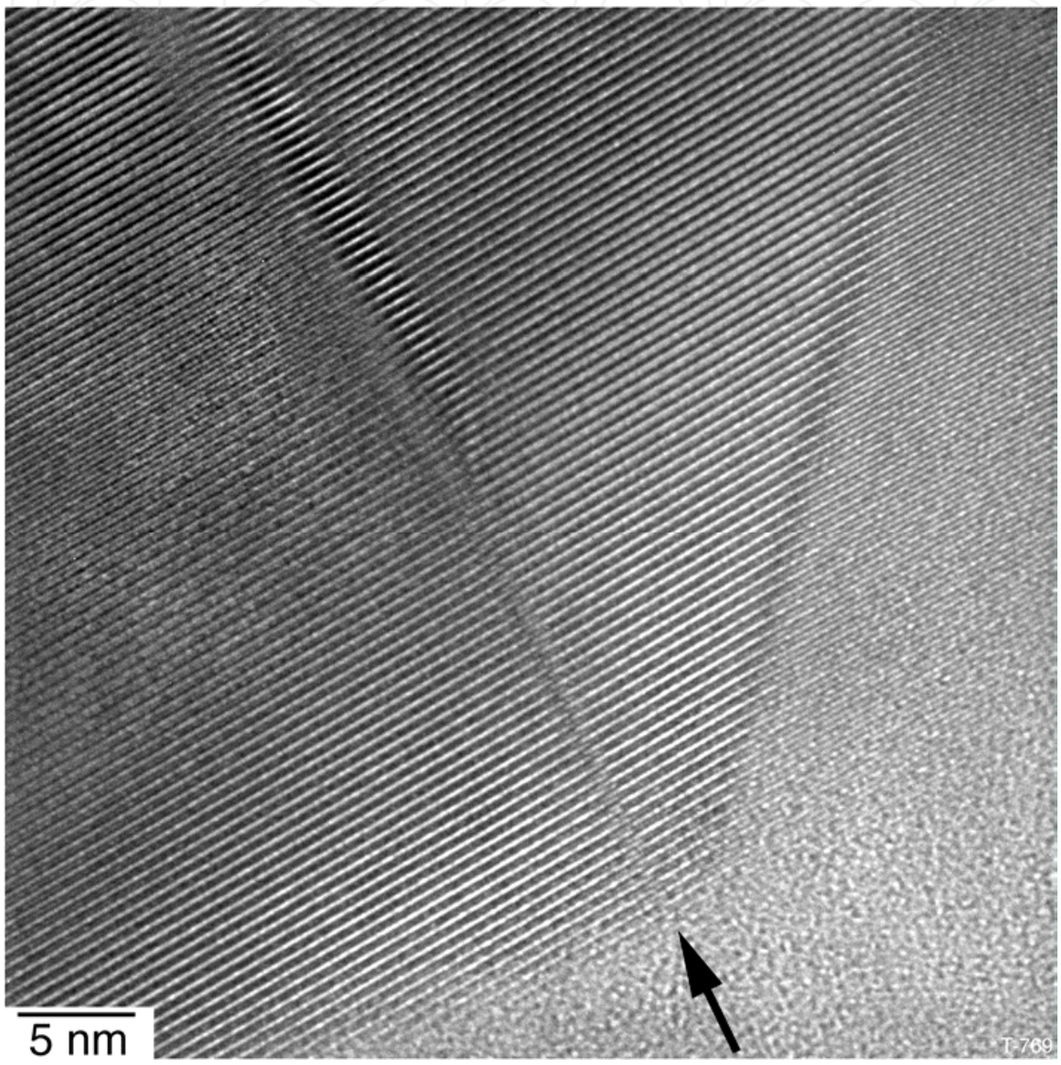

Fig. 29. An antiphase boundary (arrowed) in a crystalline grain embedded into the amorphous surface layer produced by shot peening. Experimental conditions as for Fig. 27.

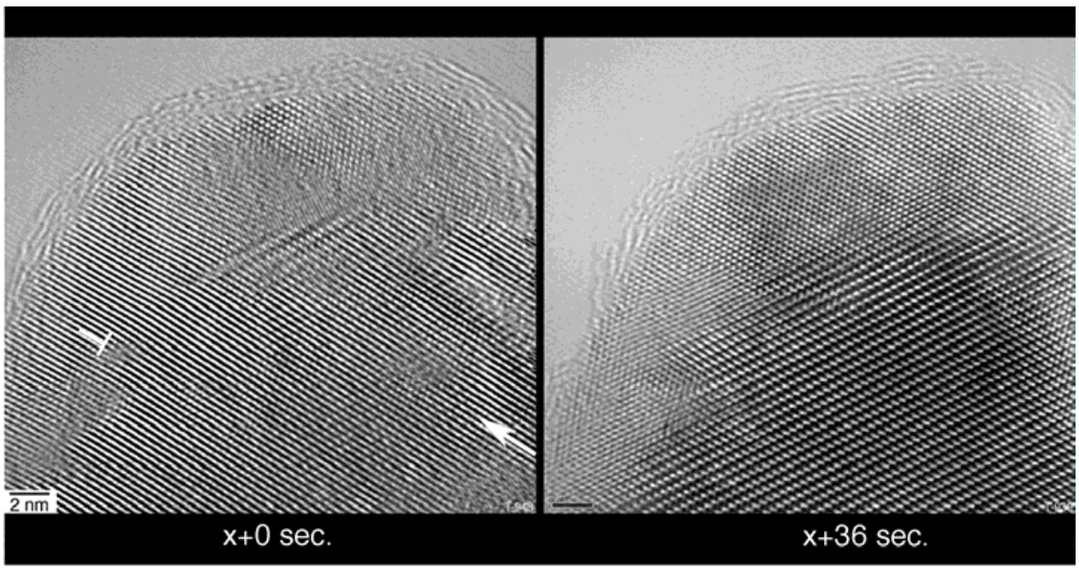

Fig. 30. Recrystallization of the crystalline surface phase observed in situ in a high-resolution transmission microscope (acceleration voltage 300 kV). Experimental conditions as for Fig. 27.

7. Conclusions

As with other metals recrystallization in multiphase titanium aluminide alloys is triggered by heterogeneities in the deformed state. However, there are several specifics that involve the following features.

The deformation heterogeneities are formed by a significant plastic anisotropy of the majority phases γ(TiAl) and α_2(Ti_3Al), twin intersections and elastic buckling of lamellar constituents.

The release of strain energy by recovery seems to be relatively easy and probably retards the recrystallization kinetics.

In the evolution of the microstructure concurrent phase transformations occur that are primarily initiated by a non-equilibrium constitution; other factors supporting phase transformations are local mechanical stresses or chemical driving pressure due contamination with gaseous elements. The combination of these effects can give rise to solid state amorphisation.

The complex interactions between deformation, recovery and phase transformation are of great importance for processing and service of TiAl alloys.

8. Acknowledgments

The author acknowledges the continuous support of St. Eggert, D. Herrmann, U. Lorenz, M. Oehring, and J. Paul, from the Helmholtz Zentrum Geesthacht, Germany. Thanks are due to Th. Heckel, A. El-Chaikh and H.-J. Christ from Universität Siegen, Germany, for performing the fatigue experiments. The financial support by the Deutsche Forschungsgemeinschaft (Projects AP 49/5 and AP 49/4-6) is gratefully acknowledged.

8. References

[1] F. Appel, J.D.H. Paul and Michael Oehring, *Gamma Titanium Aluminide Alloys - Science and Technology* (Wiley VCH, Weinheim, 2011).
[2] M. Yamaguchi, H. Inui and K. Ito, Acta Mater. 47, 307 (2000).
[3] C. McCullough, J.J. Valencia, C.G. Levi, and R. Mehrabian, *Acta Metall.* 37, 1321 (1989).
[4] P. M. Hazzledine, Intermetallics 6, 673 (1998).
[5] M.J. Blackburn, in: R.I. Jaffe, N.E. Promisel, eds. *The Science Technology and Applications of Titanium*, Pergamon, Oxford 1970.
[6] U. Fröbel and F. Appel, Acta Mater. 50, 3693 (2002).
[7] H.I. Aaronson, Metall. Trans. A, 24A, 241 (1993).
[8] F.C. Frank and J.H. van der Merwe, Proc. Roy. Soc. Series A - Mathematical and Physical Sciences A 198, 205 (1949).
[9] M.G. Hall, H.I. Aaronson and K.R. Kinsman, Surf. Sci. 31, 257 (1972).
[10] R.C. Pond, in: *Dislocations in Solids, Vol. 8*, ed. F.R.N. Nabarro (North-Holland, Amsterdam, 1989), p.1.
[11] J.M. Howe, R.C. Pond and J.P. Hirth, Progr. Mater. Sci. 54, 792 (2009).
[12] L. Zhao and K. Tangri, Acta Metall. Mater. 39, 2209 (1991)
[13] S.R. Singh and J. M. Howe, Phil. Mag. A 66, 739 (1992).
[14] S. Rao, C. Woodward and P. Hazzledine, in: *Defect Interface Interactions*, Materials Research Society Symposium Proceedings, Vol. 319, eds. E.P. Kvam, A.H. King, M.J. Mills, T.D. Sands, and V. Vitek (MRS, Pittsburgh, PA, 1994), p. 285.
[15] P. Shang, T.T. Cheng and M. Aindow, Phil. Mag. A 79, 2553 (1999).
[16] R.C. Pond, P. Shang, T.T. Cheng, and M. Aindow, Acta Mater. 48, 1047 (2000).
[17] P. Shang, T.T. Cheng and M. Aindow, Phil. Mag. Lett. 80, 1 (2000).
[18] J.P. Hirth and J. Lothe, *Theory of Dislocations* (Krieger, Melbourne, 1992).
[19] P.M. Hazzledine, B.K. Kad, H.L. Fraser, and D.M. Dimiduk, in: *Intermetallic Matrix Composites II,* Mater. Res. Soc. Symp. Proc. Vol. 273, eds. D.B. Miracle, D.L. Anton, J.A. Graves (MRS, Pittsburgh, PA, 1992), p.81.
[20] F. Appel and U. Christoph, Intermetallics 7, 1173 (1999).
[21] B. Shoykhet, M.A. Grinfeld and P.M. Hazzledine, Acta Mater. 46, 3761 (1998).
[22] F. Appel, J.D.H. Paul and M. Oehring, Mater. Sci. Eng. A 493, 232 (2008).
[23] E. Abe, T. Kumagai and M. Nakamura, Intermetallics 4, 327 (1996).
[24] R. Ducher, B. Viguier and J. Lacaze, Scripta Mater. 47, 307 (2002).
[25] A.K. Gogia, T.K. Nandy, D. Banerjee, T. Carisey, J.L. Strudel and J.M. Franchet, Intermetallics 6, 741 (1998).
[26] T. Haibach and W. Steurer, Acta Crystallographica A, 52, 277 (1996).
[27] D. Nguyen-Manh and D.G. Pettifor, in: *Gamma Titanium Aluminides 1999*, eds. Y-W. Kim, D.M. Dimiduk and M.H. Loretto (TMS, Warrendale, PA, 1999), p. 175.
[28] M.H. Yoo and J. Zou, C.L. Fu, Mater. Sci. Eng. A 192-193, 14 (1995).
[29] V. Seetharaman and S.L. Semiatin, Metall. Trans. A, 27A, 1987 (1996).
[30] Y-W. Kim and D.M. Dimiduk, in: *Structural Intermetallics 1997*, eds. M.V. Nathal, R. Darolia, C.T. Liu, P.L. Martin, D.B. Miracle, R. Wagner, and M. Yamaguchi (TMS, Warrendale, PA, 1997), p. 531.
[31] F. Appel and R. Wagner, Mater. Sci. Eng. R22, 187 (1998).
[32] Y. Mishin and Chr. Herzig, Acta Mater. 48, 589 (2000).
[33] M.H. Yoo and C.L. Fu, Metall. Mater. Trans. A, 29A, 49 (1998).

[34] Y. Minonishi, Mater. Sci. Eng. A 192-193, 830 (1995).
[35] Y.Q. Sun, P.M. Hazzledine and J.W. Christian, Phil. Mag. A 68, 471 (1993).
[36] Y.Q. Sun, P.M. Hazzledine and J.W. Christian, Phil. Mag. A 68, 495 (1993).
[37] S. Wardle, I. Phan and G. Hug, Phil. Mag. A 67, 497 (1993).
[38] J.W. Christian and S. Mahajan, Progr. Mater. Sci. 39, 1 (1995).
[39] F. Appel, Phil. Mag. 85, 205 (2005).
[40] F. Appel, U. Sparka and R. Wagner, Intermetallics 7, 325 (1999).
[41] R. M. Imayev, V.M. Imayev, M. Oehring, and F. Appel, Metall. Mater. Trans. A, 36A, 859 (2005).
[42] T. Fujiwara, A. Nakamura, M. Hosomi, S.R. Nishitani, Y. Shirai, and M. Yamaguchi, Phil. Mag. A, 61, 591 (1990).
[43] Th. Schaden, F.D.Fischer, H. Clemens, F. Appel, and A. Bartels, Adv. Eng. Mater. 8, 1109 (2006).
[44] R.A. Brockman, Int. J. Plasticity 19, 1749 (2003).
[45] J. Beddoes, W. Wallace and L. Zhao, Int. Mater. Rev. 40, 197 (1995).
[46] M. Oehring, F. Appel, P.J. Ennis, and R. Wagner, Intermetallics 7, 335 (1999).
[47] T. Furuhara, J.M. Howe and H.J. Anderson, Acta Metall. Mater. 39, 2873 (1991).
[48] S.R. Singh and J.M. Howe, Phil. Mag. Lett. 65, 233 (1992).
[49] E. Abe, S. Kajiwara, T. Kumagai, and N. Nakamura, Phil. Mag. A 75, 975 (1997).
[50] R.W. Cahn, in: *High Temperature Aluminides and Intermetallics*, eds. S.H. Whang, C.T. Liu, D.P. Pope, and J.O. Stiegler (TMS, Warrendale, PA, 1990), p. 245.
[51] F.J. Humphreys and M. Hatherly, *Recrystallization and Related Annealing Phenomena* (Pergamon, Oxford, 1995).
[52] F. Appel, U. Christoph and M. Oehring, Mater. Sci. Eng. A 329-331, 780 (2002).
[53] B. Chalmers and H. Gleiter, Phil. Mag. 23, 1541 (1971).
[54] D. Hu, A.B. Godfrey and M. Loretto, Intermetallics 6, 413 (1998).
[55] G. Hénaff and A.-L. Gloanec, Intermetallics 13, 543 (2005).
[56] F. Appel, Th. Heckel and H.J. Christ, Int. J. Fatigue 32, 792 (2010).
[57] D. Herrmann and F. Appel, Metall. Mater. Trans. A, 40A, 1881 (2009).
[58] U.R. Kattner, J.C. Liu and Y.A. Chang, Metall. Trans. A, 23A, 2081 (1992).
[59] S.P. Godfrey, P.L. Threadgill and M. Strangwood, in: *High-Temperature Ordered Intermetallic Alloys VI*, Materials Research Society Symposia Proceedings, Vol. 364, eds. J.A. Horton, I. Baker, S. Hanada, R.D. Noebe, and D.S. Schwartz (MRS, Pittsburgh, PA, 1995), p. 793.
[60] J. Lindemann, C. Buque and F. Appel, Acta Mater. 54, 1155 (2006).

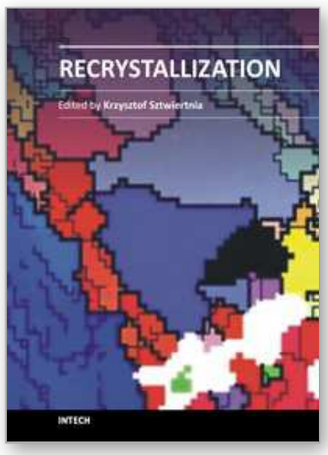

Recrystallization

Edited by Prof. Krzysztof Sztwiertnia

ISBN 978-953-51-0122-2
Hard cover, 464 pages
Publisher InTech
Published online 07, March, 2012
Published in print edition March, 2012

Recrystallization shows selected results obtained during the last few years by scientists who work on recrystallization-related issues. These scientists offer their knowledge from the perspective of a range of scientific disciplines, such as geology and metallurgy. The authors emphasize that the progress in this particular field of science is possible today thanks to the coordinated action of many research groups that work in materials science, chemistry, physics, geology, and other sciences. Thus, it is possible to perform a comprehensive analysis of the scientific problem. The analysis starts from the selection of appropriate techniques and methods of characterization. It is then combined with the development of new tools in diagnostics, and it ends with modeling of phenomena.

How to reference

In order to correctly reference this scholarly work, feel free to copy and paste the following:

Fritz Appel (2012). Phase Transformations and Recrystallization Processes During Synthesis, Processing and Service of TiAl Alloys, Recrystallization, Prof. Krzysztof Sztwiertnia (Ed.), ISBN: 978-953-51-0122-2, InTech, Available from: http://www.intechopen.com/books/recrystallization/phase-transformations-and-recrystallization-processes-during-synthesis-processing-and-service-of-tia

INTECH
open science | open minds

InTech Europe
University Campus STeP Ri
Slavka Krautzeka 83/A
51000 Rijeka, Croatia
Phone: +385 (51) 770 447
Fax: +385 (51) 686 166
www.intechopen.com

InTech China
Unit 405, Office Block, Hotel Equatorial Shanghai
No.65, Yan An Road (West), Shanghai, 200040, China
中国上海市延安西路65号上海国际贵都大饭店办公楼405单元
Phone: +86-21-62489820
Fax: +86-21-62489821

IntechOpen